Advancing the Mechanical Performance of Glasses: Perspectives and Challenges

Wondraczek, Lothar; Bouchbinder, Eran; Ehrlicher, Allen; Mauro, John C.; Sajzew, Roman; Smedskjaer, Morten M.

Published in:
Advanced Materials

DOI (link to publication from Publisher):
10.1002/adma.202109029

Publication date:
2022

Document Version
Publisher's PDF, also known as Version of record

Wiley Analytical Science

Free Virtual Conference

The 4th edition of the Wiley Analytical Science Conference starts April 26, 2022!

Join virtual seminars and connect with key experts during live Q&A sessions.

Explore the state of the art methods and advances in:

- Microscopy
- Lab Automation & Equipment
- Pharma
- Spectroscopy
- Forensics
- Food Science

Events.bizzabo.com/WASconferenceSpring22

WILEY

ADVANCED MATERIALS
www.advmat.de

Advancing the Mechanical Performance of Glasses: Perspectives and Challenges

Lothar Wondraczek, Eran Bouchbinder, Allen Ehrlicher, John C. Mauro, Roman Sajzew, and Morten M. Smedskjaer*

Glasses are materials that lack a crystalline microstructure and long-range atomic order. Instead, they feature heterogeneity and disorder on superstructural scales, which have profound consequences for their elastic response, material strength, fracture toughness, and the characteristics of dynamic fracture. These structure–property relations present a rich field of study in fundamental glass physics and are also becoming increasingly important in the design of modern materials with improved mechanical performance. A first step in this direction involves glass-like materials that retain optical transparency and the haptics of classical glass products, while overcoming the limitations of brittleness. Among these, novel types of oxide glasses, hybrid glasses, phase-separated glasses, and bioinspired glass–polymer composites hold significant promise. Such materials are designed from the bottom-up, building on structure–property relations, modeling of stresses and strains at relevant length scales, and machine learning predictions. Their fabrication requires a more scientifically driven approach to materials design and processing, building on the physics of structural disorder and its consequences for structural rearrangements, defect initiation, and dynamic fracture in response to mechanical load. In this article, a perspective is provided on this highly interdisciplinary field of research in terms of its most recent challenges and opportunities.

1. Introduction

This article aims to offer a perspective on opportunities and challenges in the design of functional glass materials with tailored mechanical performance. We will review recent advances in terms of deciphering structure–property relationships and the nonaffine nature of glass mechanical behavior, of computational and computer-assisted methods for accelerated materials discovery, and of physicochemical insight at glass formation and synthesis in unconventional types of materials. Despite this progress, significant questions remain as to the fundamental role of structural heterogeneity and its consequences for the predictability of mechanical properties underlying the many applications of glass. Today's challenge is to translate new understanding of the physics of disorder, glass chemistry, and surface mechanics into tools that enable future glass products with adapted elasticity, strength, and toughness. We will therefore consider fundamental advances in relation to emerging glass applications. While the aforementioned physical insights have mostly been obtained by computational simulation of model systems, and often through the examination of metallic glasses, we will here focus on glasses suitable for visible transparency, in particular silicate glasses, such as a representative of today's most prolific glass devices, ranging from ultrathin substrates to strong and visually transparent cover materials. We will further consider hybrid glasses and glass-like composite materials as emerging alternatives that may overcome the ubiquitous conflict between strength and toughness.[1]

L. Wondraczek, R. Sajzew
Otto Schott Institute of Materials Research
Friedrich Schiller University Jena
Fraunhoferstrasse 6, 07743 Jena, Germany
E-mail: lothar.wondraczek@uni-jena.de

L. Wondraczek
Center of Energy and Environmental Chemistry Jena (CEEC Jena)
Friedrich Schiller University Jena
Philosophenweg 7, 07743 Jena, Germany

The ORCID identification number(s) for the author(s) of this article can be found under https://doi.org/10.1002/adma.202109029.

DOI: 10.1002/adma.202109029

E. Bouchbinder
Chemical and Biological Physics Department
Weizmann Institute of Science
Rehovot 7610001, Israel

A. Ehrlicher
Department of Bioengineering
McGill University
Montreal H3A 2A7, Canada

J. C. Mauro
Department of Materials Science and Engineering
The Pennsylvania State University
University Park, PA 16802, USA

M. M. Smedskjaer
Department of Chemistry and Bioscience
Aalborg University
Aalborg 9220, Denmark

Mechanical performance remains a primary design target in modern glass technology, given the relatively low strength levels currently accessible in practical applications. There has been a consensus that stress amplification and brittleness (which limit the achievable levels of practical strength) cannot be overcome by conventional means.[2] Yet, a number of recent discoveries strongly motivate the further search for tools that would enable glasses with improved mechanical behavior—from glass physics and the fundamental understanding of disorder to glass chemistry, accelerated materials discovery, and a strongly improved view of the structural rearrangements that underlie the mechanical response of glasses at different length scales.

The past decade has seen a broad variety of glass applications that have been made possible by the enhancement of mechanical performance, be it through materials chemistry, (post-) processing, or combinations thereof. For example, strengthened glass covers for handheld electronic devices have reached unprecedented levels of damage resistance and have even become foldable.[3] As another example, roll-to-roll processing of ultrathin and flexible glass substrates has been made possible;[4,5] advanced dicing and postprocessing techniques have led to defect-free and, thus, strong edges to withstand bending loads.[6,7] Thermal tempering has been enabled for thin-walled glass products,[8] usable in glass–glass solar modules, flexible mirror substrates, quadruple-glazing, and lightweight glass containers. Optical fibers with enhanced bending resistance (both mechanical and in terms of optical loss) are used for fiber-to-the-X as well as short-haul light transmission techniques, or even suggested for integration as a functional component within textile structures.[9]

At the same time, these and other areas of glass applications remain limited by the restrictions of glass brittleness and surface defect propensity. Furthermore, various areas of glass application for which mechanical performance has been a less stringent restriction in the past are now experiencing higher demands in terms of material strength, reliability, and defect resistance. Sometimes this may be due to the more widespread use of glass products, for example, in direct, haptic user interaction (e.g., interactive displays, smart glasses, or textile structures). It may also be driven by new levels of functionality and safety requirements (e.g., smart windows,[10] but also pharmaceutical packaging[11]), sustainability goals (lightweight objects with reduced embodied CO_2, enhanced service life), upscaling efforts (e.g., chemically strengthened glass products, larger and/or thinner windows or other glass structures in architecture), or emerging applications of specialty glasses. For example, glasses with adapted mechanical performance are expected to play important roles in 5G and mm wave technologies,[12] as membranes for gas separation,[13,14] or as microscale objects[15] such as in glass-based microfluidic reactors and sensor components or capillary devices. This holds in similar ways for the many other areas, in which glasses are indispensable components.

Given the full breadth of the topic, we will focus here on the material prospects and challenges en route to functional glasses with adapted mechanical performance (Section 2). We will start from the question of how glassy disorder and microscopic non-affinity in the response to mechanical stimulation contribute to the observable (macroscopic) mechanical performance, and to which extent our recent understanding based on model glasses can potentially be transferred to the real world (Section 3). Considering the prominent role of bendable and flexible glass substrates (and glass fibers) in functional devices and further emerging applications, we will briefly address glass bendability and the tailoring of elastic properties beyond classical limits (Section 4). We will also discuss the practical aspects of surface defect propensity, including state-of-the-art experimental methodologies from quasi-static to ultrafast testing, with a focus on dynamic failure (Sections 5 and 6). Computational tools, their role in the accelerated material discovery, and their limitations and challenges in terms of studying glass mechanics are the topic of Section 7.

With these overarching questions in mind, research into new materials, material fabrication processes, and postprocessing methods aims for glasses with adapted stiffness and elasticity, reduced surface defect propensity, enhanced fracture toughness, safety of operation and, eventually, secondary functionality. We expect that future progress in these areas will provide versatile opportunities far beyond the above applications; to this end, we will consider three primary research directions into novel kinds of glass materials, from recent advances in oxide glass chemistry to hybrid glasses and bioinspired glass-like composite materials (Section 8).

A scholarly review of the mechanical properties of oxide glasses is provided in ref. [16]. For metallic and chalcogenide glasses, readers are referred to refs. [17,18], respectively. While we will point to the importance of environmental (extrinsic) effects on glass strength, we will not go into detail in relation to stress corrosion.[19,20] Finally, here we will not review the broad field of postprocessing and strengthening methods of glass products beyond their relevance for glass frangibility, fracture toughness, tailoring of structural disorder and—as a general note—defect propensity. A recent account of this subject area is provided in ref. [21]. Specifically on coatings, we refer the readers to refs. [22–26].

2. Brittleness, Intrinsic Strength, and Defect Propensity of Silicate Glasses

Ideally, brittle fracture involves a sequential bond rupture with limited spatially extended dissipation; the intrinsic strength of glasses is therefore related to the energy required for bond cleavage, which in turn is affected by local strain.[27] Reactive chemical species near the site of defect initiation and growth may strongly influence the local energetics. For example, in the presence of water molecules, the activation energy of Si—O bond cleavage in silica glass reduces from the homolytic dissociation energy of 624.0 to 163.0 kJ mol^{-1}.[27] While the intrinsic strength is therefore given by the structure and chemical composition of the glass itself,[28] the practical (experimental) strength is usually very strongly dependent on extrinsic factors such as the environment of observation and the presence of surface flaws and defects. Reactive crack propagation resulting from interactions of the glass network with environmental species (most prominently, water molecules) is understood as a corrosion process that leads to sub-critical failure. Excellent reviews of the present state of knowledge on this field are

provided in refs. [19,20]. However, beyond the classical model of Michalske and Freiman,[29] the specific chemical reactions occurring at the crack tip remain unclear. This is particularly the case in the chemically more complex silicate glasses, in which mobile glass constituents (such as alkali ions[30]) and environmental or condensate species[31] interact at the crack tip, forming an intricate reaction space whose chemical details are presently unknown.[32] On this line, very recent efforts to incorporate reactive water species directly into the glass matrix (as opposed to their uncontrolled environmental presence) present an interesting path towards a new class of glasses with controllable crack tip chemistry and, thus, defect propensity.[33,34]

If environmental effects are reduced to the best possible degree, for example, by performing strength tests on pristine, nearly flawless materials, in vacuum and at low temperature, strength values in the range of 10 GPa are observed for common silicate glasses.[35] When micro- or nanoscale samples are studied, the size and frequency of surface flaws or structural defects can be further reduced, providing another means to approach intrinsic strength levels in experiments.[36] Similarly, techniques that enable observations at small length scale hold promise for extracting intrinsic data.[37,38] For example, instrumented indentation using a wedge on glass fiber can provide information on surface crack initiation in good agreement with tensile strength testing.[37] Evaluating the surface sink-in during lateral indentation with a blunt indenter was demonstrated as a means to evaluate the yielding of glass surfaces.[38,39] A major advantage of such methods lies in their applicability to real-scale samples, i.e., specimens that do not require microfabrication or further processing, affecting subsequent data evaluation and interpretability. Despite such advances, the availability of intrinsic data is still limited to only a small number of glass compositions, which presents a serious obstacle in the elucidation of the effect of glass chemistry and atomic structure on glass mechanics versus the role of extrinsic factors. This holds, particularly for low-temperature/low-pressure (inert) studies. Recent experiments on the dynamics of vacuum cracking seem very timely in this regard.[40]

Bond rupture and cracking generally occur as a result of stress amplification;[41] presumably, the homogeneous stress field accompanied by a tested glass sample fails to reach a level at which cooperative structural rearrangements and bond switching reactions are initiated.[42] Instead, localized structural rearrangement and, ultimately, bond rupture lead to defect growth and, hence, further stress amplification. The critical stress σ_c at which a glass fails can be described through either fracture toughness K_c (K_{Ic} in the case of mode I fracture) or fracture energy Γ (see also Section 6), and it is a direct result of a combination of the material's elastic constants, the fracture surface energy and the inverse of the pertinent flaw size $\sqrt{c}$, leading to stress amplification. For example, using the homolytic bond dissociation energy of silica and an interatomic distance equaling the Si—O bond length of ≈0.14 nm, a stress value of ≈40 GPa is estimated. Vitreous SiO_2, however, is comprised of a network of rings of SiO_4 tetrahedra, so that a more appropriate assumption for the intrinsic defect size would be the size of the voids within these rings,[43] reducing the estimated intrinsic strength to around 20 GPa—a value which has been approached experimentally using defect-free silica nanowires (**Figure 1**a).[36] From such understanding, glasses with higher packing density would appear to facilitate plastic deformation, such as in bulk metallic glasses in which plastic deformation is mediated through pronounced shear transformation zones (STZs,[17,44]). Indeed, Frankberg et al.[45] demonstrated that flawless films of amorphous alumina with a substantially higher packing density as compared to that of silica can exhibit high tensile ductility (Figure 1b). They reported an up to 25-times higher probability of bond switching reactions in this case, owing to the built-up of a homogeneous stress field, reaching the threshold level for such reactions.[45]

Interestingly, the structure of glasses depends not only on their chemistry but also on their thermo-mechanical history, that is, the cooling rate and the pressure applied when producing the glass from its parent liquid;[46] we will discuss in the following section how this dependence may lead to vast variations in the fundamental response of a glass to mechanical stimulation (see

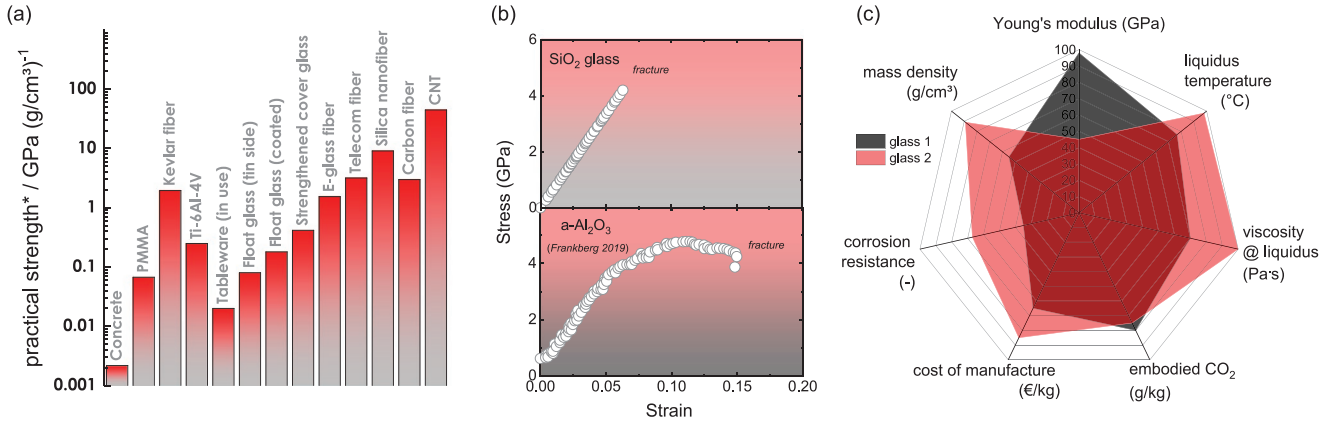

Figure 1. a) Magnitudes of specific practical strength typically observed for a range of materials, including various glass products. The upper limit of glassy silica nanofiber is taken from ref. [36] The reported strength values are for uniaxial tensile testing, except for the flat glass data, for which ring-on-ring values are given. A value reported for carbon nanotubes (CNT) is shown for further comparison.[53] b) Stress–strain curve of bulk silica glass under tensile load, and of a ductile nanoscale layer of amorphous alumina (data in panel (b) reproduced with permission.[42,45]). c) Qualitative property matrix, shown by way of example for the selection of glass candidates for high-modulus reinforcement fiber.

Section 3). Initially, it is clear that also brittleness and defect propensity depend on glass formation history. Indeed, it was suggested for a broad range of chemistries that the observable strength of a glass is related to its configurational energy and the temperature itself at which the glass transition occurred,[47] although the specific relations might be nonintuitive because of opposing interdependencies between bond switching and compaction reactions. For example, while higher packing density—such as achieved by slower cooling[48] or cooling under pressure[49]—would facilitate plastic deformation in principle, it was also found that rejuvenation by rapid quenching facilitates material deformation through structural compaction, leading to higher defect resistance.[8,50] Furthermore, additional p,T-dependent reactions may occur, such as the tetrahedral-to-trigonal coordination transition of borate species.[51] In the case of borate-containing glasses, such reactions may significantly reduce the stress threshold for shear deformation.[52] However, the practical potentials of tailoring glass strength, brittleness, and defect propensity through fictive temperature (and fictive pressure) remain unclear. As we will discuss in Section 3, this aspect represents one of the fundamental features of glassy materials, hence, future studies which connect model understanding and real-world opportunities are of great interest.

Due to the presence of defects, the practical strength of glass products varies over several orders of magnitude (Figure 1a), while the glass's chemical composition is of only minor importance.[2] However, a change of paradigm occurred in the early 2000s, when Sehgal and Ito reported that even slight changes of glass composition may have pronou nced consequences for the formation of surface defects under sharp contact load, the glass's defect propensity.[54] This stimulated major research efforts, which have turned—over the past decade—into one of the most prolific areas of glass research: mostly using instrumented indentation testing, the aim is to elucidate the reactions governing contact energy dissipation by local plastic deformation (over cracking) and their dependence on glass composition. For (apparently) equally brittle glass compositions, it was found that their reaction to sharp contact loads may differ significantly, leading to versatile defect patterns which depend on the type of glass and the specific testing conditions (**Figure 2**). These defect patterns represent the different routes of stress built-up and dissipation, which are affected by material composition. The assumption was made that defect-resistant glasses may be discovered through tailoring the material's ability to (locally) densify or shear (see Section 8); for recent reviews on this subject, see refs. [55–57]. It is, however, presently unclear to which extent such laboratory experimentation is able to mimic real-world situations of surface damage. As a consequence, the transfer of lessons learnt from recent microscale indentation methodology (often supported through computational simulation, see Section 7) to novel glass products is only at its beginning.

3. Glassy Disorder, Elastic Properties, and Fracture Toughness

As indicated in Section 2, the intrinsic nonequilibrium nature of the glassy state of matter implies that glasses, even of the same composition, may feature significantly different properties: while elastic properties may vary only within relatively small ranges, a glass of the same composition might—in principle—be either ductile or brittle. The origin of this variability is the multiplicity of disordered structures that glasses can be attained as a function of their chemical composition, fictive temperature, and fictive pressure. Consequently, a major challenge in glass science is the quantification of glassy disorder and understanding its effect on the emerging macroscopic properties. In particular, understanding the relations between glassy disorder and the mechanical properties of glasses—, e.g., stiffness, strength, and fracture toughness—is of prime importance. Developing our knowledge of such structure–properties relations is not only central from a fundamental perspective, but also crucial for conceiving novel processing and chemical design routes towards improved mechanical performance. As noted in the previous paragraphs, this could significantly broaden the range of glass applications. The problem at hand is that the primary tool for property prediction used for crystalline materials—lattice symmetry—is not available for glasses. For example, this means that one cannot precisely predict bond energy density in straightforward ways. Furthermore, disorder leads to spatially fluctuating elastic constants, resulting in nonaffine deformation as a function of observation length.[58,59] Due to the inability to quantify this behavior, practical predictions of the mechanical properties of glasses have relied on empirical or sometimes semiempirical regression methods for more than a century,[60,61] and even the more recent efforts to introduce machine learning for glass property predictions have as of yet achieved only little progress toward building new physical insights[62] (see Section 8 for a further discussion on the state-of-the-art regarding glass property design).

Disorder endows glassy materials with universal properties, for example the temperature dependence of the thermal conductivity and the specific heat in the low-temperature regime,[63] the Boson peak in the reduced vibrational density of states (VDoS),[64] localized immobile rearrangements (STZs) that mediate plastic deformation in metallic glasses,[65] and the phenomenon of "nanoductility" in silicate glasses.[66] Recent progress has shed new light on both the emergence of universal glassy behaviors and on the quantification of a specific state of disorder, as well as on the relations between the latter and a broad range of mechanical properties. It has been shown, using molecular dynamics (MD) simulations, that glasses generically exhibit low-energy excitations that are not spatially extended, but rather feature spatial localization on a scale of a few atomic distances in linear size.[67,68] Moreover, these low-energy glassy excitations have been shown to follow a universal non-Debye vibrational density of states (VDoS) $D(\omega) \sim \omega^4$,[67–70] where ω is the angular vibrational frequency, as suggested since the late 1980s;[71,72] however, as of today, such insights remain largely limited to model glasses.

Examples of the ω^4 VDoS of glassy excitations are presented in **Figure 3**a for four different computer glass models. These include: i) the Stillinger-Weber network glass-former, which employs a three-body term in the potential energy that favors tetrahedral structures, ii) a triatomic OTP-like molecular glass former, which corresponds to the Lewis-Wahnström model for the fragile glass former ortho-terphenyl (OTP), iii) a polymeric glass-former, which corresponds to soft beads connected by

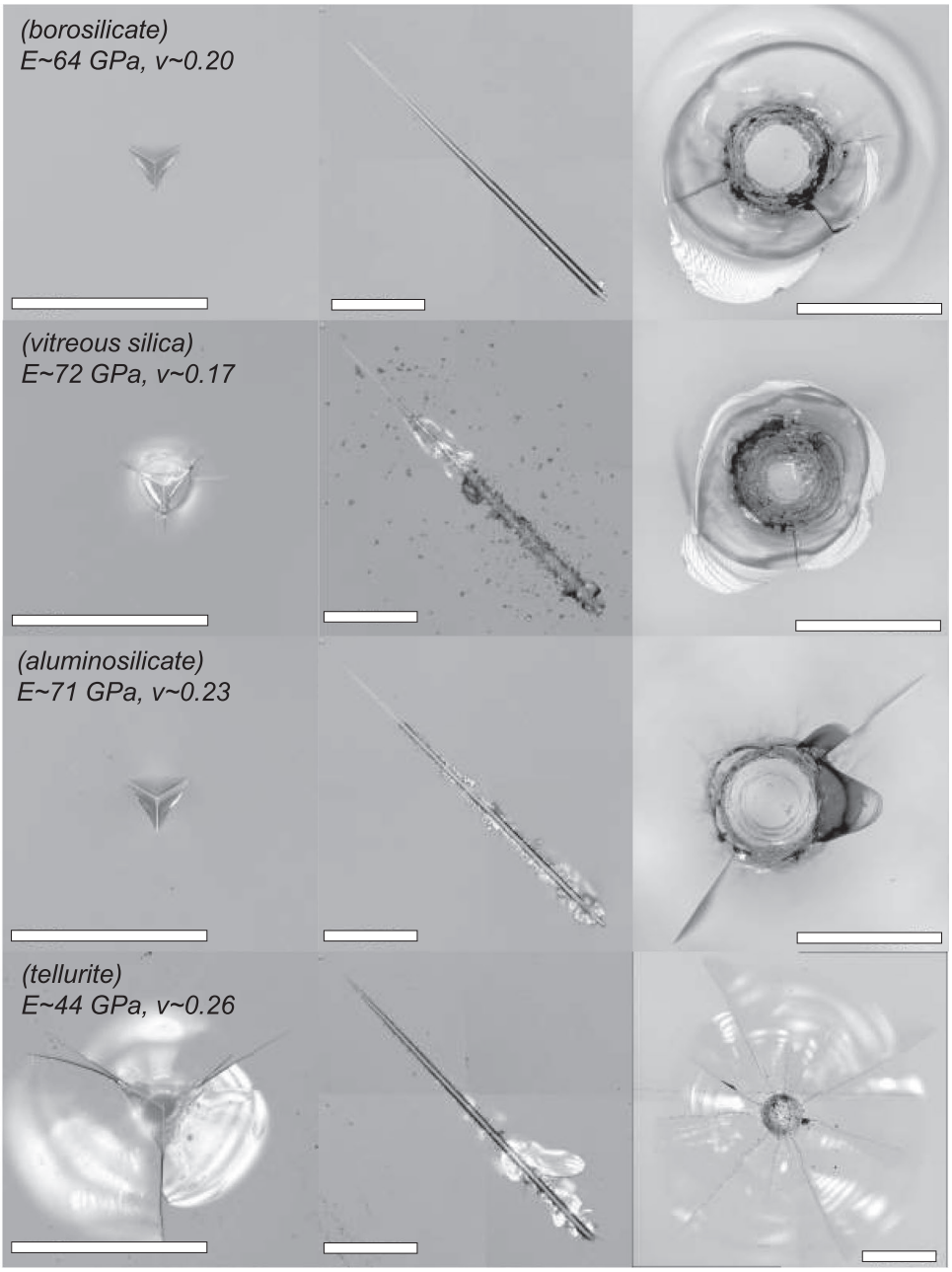

Figure 2. Various types of defects artificially produced on glass surfaces. From left to right: sharp Berkovich diamond indentation (1.962 N, 10s loading time), scratching with a spheroconical tip with a tip radius of 5 µm, and impact damage using a 500 µm ball tip, respectively. Defects are shown for four different glasses, from top to bottom: a low-alkali borosilicate glass (Boro33), vitreous silica, an aluminosilicate glass representative for display cover applications, and a tellurite glass. Young's modulus (E) and Poisson's ratio (ν) of the glasses are given. The scratch data depict ramp-load tests conducted with 50 µm s^{-1} tip velocity to variable maximum load in order to remain within the spherical regime of the tip, i.e., 350 mN for the borosilicate, 300 mN for vitreous silica, 250 mN for the aluminosilicate, and 100 mN for the tellurite glass. For the impact test, impact energies were at ≈50 mJ (silicates) and ≈5 mJ (tellurite), respectively. The scale bars are 100 µm (for Berkovich imprints and scratch grooves), and 500 µm (for impact defects), respectively.

finite extensible nonlinear elastic nonlinear springs, iv) a CuZr bulk metallic glass, which corresponds to a binary alloy composed of copper (Cu) and zirconium (Zr) atoms according to $Cu_{46}Zr_{54}$ and where the interactions are calculated using the embedded-atom method, giving rise to a spherically symmetric, many-body potential.[70] In Figure 3a, small computer glass samples have been employed in order to avoid hybridization/mixing with low-frequency phonons, which has hampered a clean identification of the ω^4 VDoS for a long time.[67,68] This presents an interesting example that for some purposes, the limited sizes of computer glasses may in fact be advantageous (see Section 7 for further details).

The universal non-Debye ω^4 VDoS implies that glass-specific properties are embedded in the prefactor A_g, defined through D

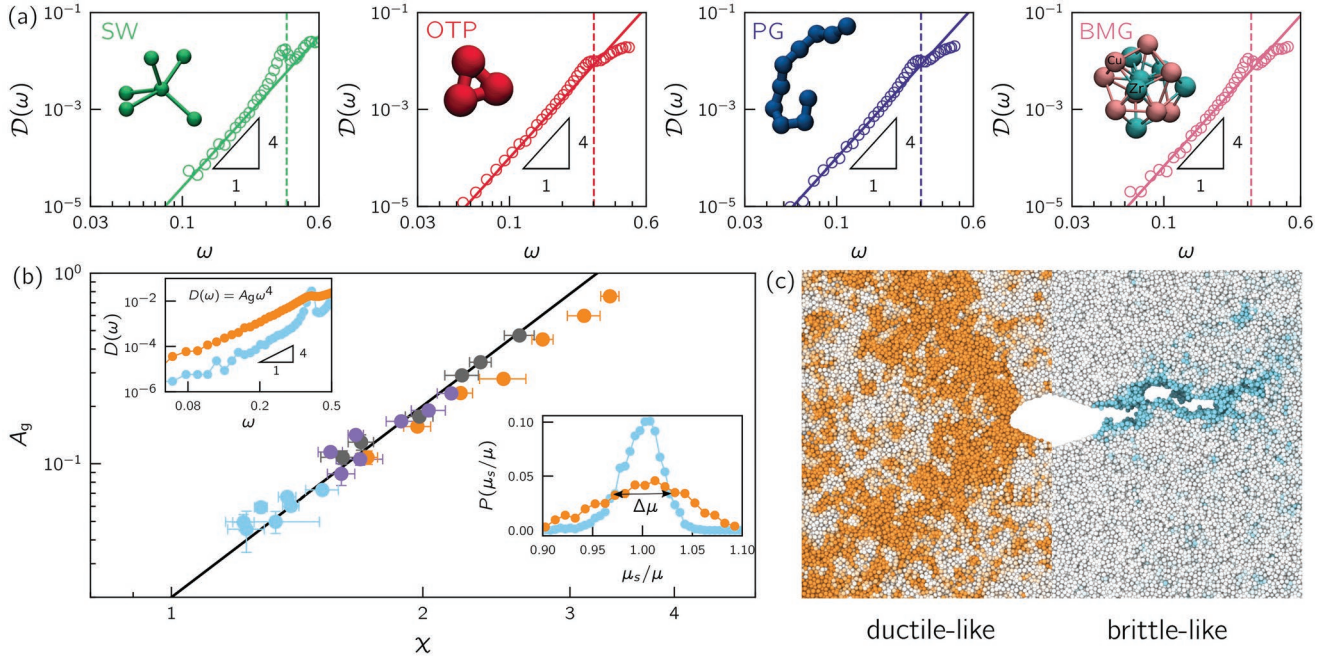

Figure 3. a) Vibrational density of states (VDoS) measured in realistic computer glass models (SW stands for the Stillinger-Weber network glass-former, OTP stands for a triatomic OTP-like molecular glass-former, PG stands for a polymeric glass-former and BMG stands for a CuZr bulk metallic glass, see text for additional details). The solid lines indicate $D(\omega) = A_g\omega^4$, clearly observed below the first phonon frequency (dashed vertical lines).[70] b) A_g versus χ, a quantifier of elastic heterogeneity of glasses, for various simple computer glasses (different colors correspond to different inter-atomic potentials, see ref. [75] for details). The data indicate a power-law relation of the form $A_g \approx \chi^{10/3}$ (insets). The shear modulus distributions (bottom-right), $P(\mu_s/\mu)$, for two computer glasses whose VDoS is shown (top-left). The distributions are obtained by calculating the shear modulus of many realizations of glasses composed of N particles each.[77,75] μ is the mean of the distribution, $\Delta\mu$ is its width (a measure of the fluctuations) and χ is defined as $\chi \underline{\underline{def}} (\Delta\mu/\mu)\sqrt{N}$.[77,75] c) Snapshots of the nonaffine plastic deformation (darker color represents more intense plastic deformation) during fracture tests with an initial diamond-shaped crack for ductile-like (left) and brittle-like (right) failure. The color code used follows that of the insets on panel (b), such that ductile-like failure (orange) corresponds to the larger A_g and the wider μ distribution (larger χ), and brittle-like failure (cyan) corresponds to the smaller A_g and the narrower μ distribution (smaller χ). a) Reproduced with permission.[70] Copyright 2020, American Physical Society. b,c) Reproduced with permission.[75] Copyright 2021, The Authors, under exclusive license to the Materials Research Society.

$(\omega) = A_g\ \omega^4$, which can serve as a quantifier of glassy disorder once properly nondimensionalized.[73] A_g is analogous to the prefactor A_D in Debye's VDoS for phonons, $A_D\omega^2$, but for glassy (nonphononic) excitations. Through computational studies, A_g has been shown to vary dramatically as a function of the glass preparation protocol, by several orders of magnitude,[73] using advanced glass-forming algorithms that allow extremely deep supercooling (comparable or even surpassing laboratory supercooling).[74] A_g has also been shown to be related to macroscopic mechanical properties such as Poisson's ratio ν[75] and to contain information about the number of soft spots,[73] i.e., spatial regions with extraordinarily low resistance to shear deformation, and as such is expected to be also related to the level of elastic heterogeneity. Elastic heterogeneity plays a central role in various approaches that aim at explaining basic glass phenomena, such as sound attenuation and the Boson peak.[76,77] Recently, a systematic approach for quantifying elastic heterogeneity in computer glasses—based on the fluctuations of the shear modulus μ —has been developed,[77] as demonstrated in the inset of Figure 3b. The resulting dimensionless measure of elastic heterogeneity χ is defined as $\chi \underline{\underline{def}} (\Delta\mu/\mu)\sqrt{N}$,[77,75] where μ is the mean of the distribution, $\Delta\mu$ is its width (a measure of the fluctuations) and N is the size (particles number) over which the fluctuations are probed. χ has been shown to systematically vary with A_g, as demonstrated in Figure 3b. Similar efforts to classify disorder in real-world glasses are ongoing.[78]

The effect of varying A_g or χ on nonlinear and dissipative glass properties, most notably on the glass damage-tolerance capabilities as quantified by the fracture toughness, is of prime importance. As A_g quantifies the number of soft spots in a glass, which have been shown to be the loci of plastic rearrangements (STZs),[79] we expect A_g—and hence also χ—to play decisive roles in the damage tolerance of a glass. The latter is intrinsically related to the ability of a glass to mitigate stress concentration at defects through plastic deformation. In fact, A_g/χ may control a transition from a damage-tolerant, ductile-like response (Figure 3c, left part) to a catastrophic failure, brittle-like response (Figure 3c, right part). This question is particularly interesting in the context of metallic glasses, where earlier works provided some evidence indicating that there might exist a critical Poisson's ratio for a brittle-to-ductile transition,[80] presumably offering an important practical guiding principle for selecting tougher glasses. Also for silicate glasses, experimental indications are available which relate structural disorder to deformation behavior;[81] however, neither quantitative details nor universality have been demonstrated to date.

Very recently, some new light has been shed on the interplay between Poisson's ratio ν and the disorder quantifiers

A_g and χ in affecting the toughness of model glasses.[75] It has been shown that ν mainly plays an extrinsic role in the toughness of glasses, i.e., when a glass can undergo Poisson's contraction under tensile loading, ν provides a measure of the relative magnitude of tensile and shear deformation, where plastic deformation is mainly sensitive to the latter.[82] Consequently, the linear response coefficient $\nu(\chi)$ affects the fracture toughness indirectly through its effect on the geometry of deformation, along with the intrinsic effect of A_g/χ. Indeed, it has been shown that the brittle to ductile transition is not characterized by a critical ν, but rather by a curved line in the χ–ν parametric plane, in a situation where Poisson's contraction is free to take place.[75] When constrained tensile loading is applied—where Poisson's contraction cannot take place—the fracture toughness has been shown to be controlled by the intrinsic effect of A_g/χ.[75] Related experimental developments using a thermoplastic forming methodology have been combined with a significantly improved ability to control the initial non-equilibrium state of a glass (quantified by the fictive temperature) and enabled very accurate measurements of the fracture toughness, demonstrating such brittle-to-ductile transitions in various metallic glasses[83] The incorporation of these ideas, e.g., regarding the number of soft spots and its evolution with plastic deformation, into macroscopic theories of glass deformation may lead to enhanced predictive powers. In particular, it may offer new avenues for relating glassy disorder to the emerging macroscopic mechanical properties.

4. From Stiff to Bendable and Flexible Glass Products

While the selection of a certain glass composition for a certain application depends on a number of factors (Figure 1c), elasticity and stiffness are of prime importance in most applications of advanced glass devices. For example, automotive glazing requires rigidity and acoustic performance presently not available from lightweight alternatives.[84] Creating hard, yet flexible, glasses currently push strategies to very thin sheets (**Figure 4**), or to composites that incorporate ductile phases, often drawing from bioinspiration as discussed in Section 8. Such bendable glasses have been demonstrated as serious alternatives for plastic substrates (e.g., polyimides[85] used in large-scale transparent and flexible OLED displays). In these applications, inorganic glass substrates do not only offer a unique set of physical properties; they are also a greatly more sustainable solution.[86]

Bending exerts stress, which must be accommodated by the glass material. Hence, high-strength glasses are sought, and bending stress needs to be kept low (for high flexibility) or high (for high stiffness). This reduces the available toolbox to the tailoring of the elastic constants (Young's modulus and Poisson ratio), installing residual stress to counteract bending loads (see Section 5) and reducing material thickness. Thereby, material thickness is the major parameter; at sufficiently low diameter, virtually any fibrous material becomes bendable.[87] For example (**Table 1**), in architectural glasses, bending (e.g., caused by a pressure drop between the window's exterior and cavities in double or triple glazings) is undesired, but low sheet

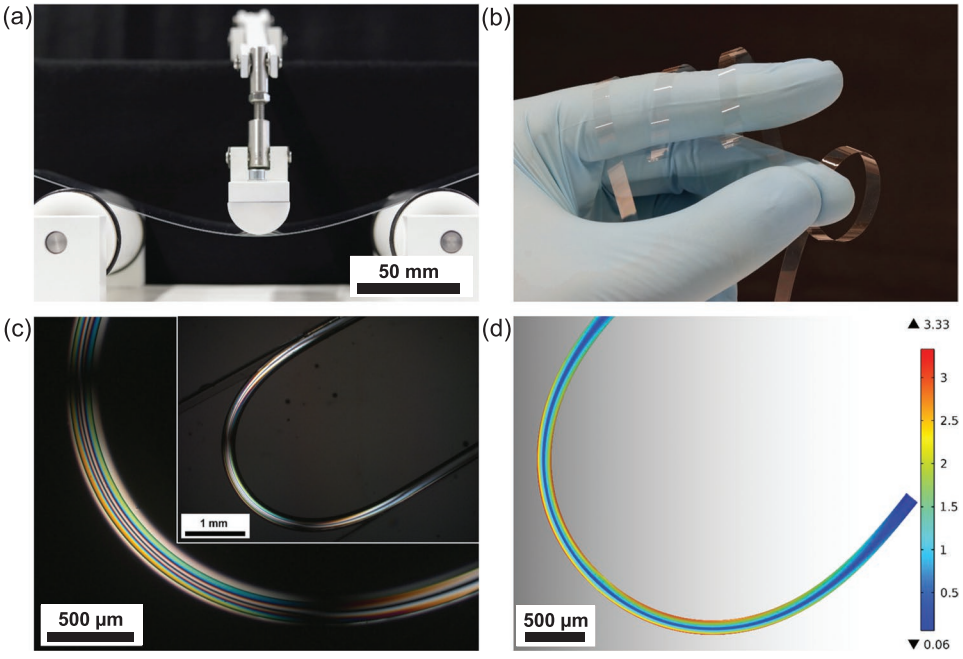

Figure 4. Bendability of silicate glasses. a) Three-point-bending of a chemically strengthened alkali aluminosilicate glass sheet with a thickness of 0.7 mm. b) Ultrathin silicate glass ribbon (NEG, thickness 20 µm, width ≈ 5 mm). c) Bent SiO_2 glass fiber with 125 µm diameter in a two-point bending setup (inset). The acrylate coated fiber was immersed in glycerol–ethanol mixture and investigated through a microscope with crossed polarizer configuration, revealing stress-induced birefringence. d) Finite element simulation of a SiO_2 glass fiber in two-point bending with indicated stress distribution and maximum stresses around the apex.

Table 1. Examples of bendable or flexible glass geometries. Values represent practical ranges. The stated bending radius is an estimate for a bending stress of 10^2 MPa.

Example	Bending radius	Approximately glass thickness or diameter
Architectural windows	≈m	2–6 mm
Dynamic reflectors	<1 m	<2 mm
Bendable display covers	<0.5 m	<1 mm
Roll-to-roll processing	≈cm	<100 µm
Telecommunication fiber/ FTTx	≈cm	<300 µm
Textile-integrated optical fiber	≈cm	<200 µm
Foldable displays	≈mm	<50 µm
Flexible glass ribbon	≈mm	3–50 µm
Fiberglass fabric, yarn	≈mm	3–20 µm
Glass wool	≈mm	3–20 µm
Silica nanofiber	<0.2 mm	<1 µm
Lightsail (hypothetical)	<0.1 mm	<0.5 µm

thickness (<4 mm) would reduce the weight of windows and, thus, their embodied energy and cost of installation. Hence, residual stress induced by thermal tempering can be used to counteract bending. Glass sheets with a thickness of 50 µm were reported as a substrate material for roll-to-roll processing of the top electrode for large area, flexible OLED lighting.[88] When the thickness is further reduced, glass substrates become highly bendable. For example, glass ribbon made by thermal drawing has achieved a present record of 3 µm in thickness,[89] leading to an achievable bending radius in the range of only a few hundred µm. Further thickness reduction to the sub-µm range would enable glass substrates with a specific weight of <1 g m^{-2}, for example, such as in the specifications of the hypothetical light sail.[90] Some less hypothetical applications involve thin glass membranes, for example, for gas separation or storage.[13,14] Aside from the manufacturing technology for achieving these very low thickness specifications, the edge strength resulting from cutting, dicing, and other post-processing methods remain a major bottleneck.[91,92] Furthermore, a trade-off exists between glass thickness and frangibility, see following Section 5.

5. Frangibility of Glasses

For an ideally brittle, nearly linear elastic material (such as, by approximation, vitreous silica), increasing the rupture stress means a concomitant increase (with slope E) in the amount of stored energy, which is released upon fracture (see Figure 1b). Hence, increasing strength levels inevitably lead to increasingly complex fracture patterns, as individual fracture planes cannot accommodate the accelerated rate of energy release. Understanding the formation and energetics of such dynamic fracture patterns is crucial for designing glasses with modified fracture toughness and cracking behavior, for example, for more robust glass devices, or for objects which break in controlled ways. There are two common (practical) tools available for such tailoring, which both address the rupture stress of glass without changing its chemical composition: as noted in Sections 2 and 3, microscopic flaws and defects (or structural disorder as affected by glass history) control local stress amplification and, hence, the strength of glass. In **Figure 5**, we show the fracture surface of an optical-grade silica glass fiber, generated under tensile loading at variable loads through introducing a surface defect by in situ wedge indentation. The fiber accompanies higher load before fracture when the wedge defect is smaller, leading to higher energy release at failure (from left to right). When cleaving the optical fiber (or, similarly, employing fracture reactions in glass cutting or dicing), a smooth, well-controlled fracture surface is desired. In turn, the quality of the fracture surfaces or edges determines the usable strength of the obtained glass object and the required intensity of post-processing, for example, by polishing.

Other than controlling the flaw or defect size, the introduction of residual stress is an established means to enhance the usable strength levels of glass products.[2,21] Most prominently, thermal and chemical tempering processes enhance the practical strength of glass articles by installing a layer of compressive stress at their surfaces. To satisfy the force balance

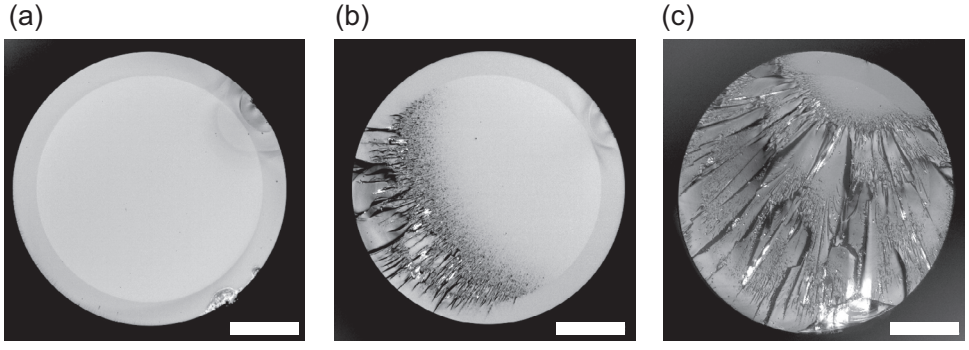

Figure 5. Fracture surface of silica optical fibers (the somewhat darker ring is a fluorine-doped silica cladding having a lower refractive index than the vitreous silica core). Fracture surfaces were generated by tensile cleaving, using a wedge placed perpendicular to the fiber axis (upper right region of fiber surface), and a uniaxial tensile stress for breaking the fiber. The wedge generates a surface defect, defining the stress at which the fiber fails under tensile load (a: 250 gf; b: 500 gf; c: 1000 gf). The differences in the fracture patterns reflect the increasing fracture energy, accompanied by increasingly unstable crack propagation. The scale bars are 50 µm.

condition, the integrated compressive stress must be balanced by an equivalent amount of integrated tensile stress in the interior of the glass.[93] The magnitude of this tensile stress is denoted as the central tension (CT), which has a large influence on the fragmentation behavior upon failure.[94] A tempered glass article is generally safe from fracture as long as surface cracks are contained within the compressive stress layer. However, once a crack penetrates through the compressive layer and into the tensile region, the tempered glass will experience spontaneous fracture as the stored tensile energy is released from the interior of the glass.[95] In practical terms, this tensile energy acts to accelerate the propagating crack until it reaches its terminal velocity. The terminal velocity of the crack is related to elastic wave velocities of the glass and to dynamic instabilities; for typical silicate glasses, the terminal velocity is on the order of 2 km s^{-1}.[96] The details of this process have been studied through combinations of physical experimentation and computational simulation using model glasses; their understanding is a crucial prerequisite for the knowledge-based design of glasses with specific fracture dynamics, as will be discussed in the following Section 6. For the moment, we simply state that such crack branching enables a higher release rate for the stored tensile energy from the interior of the glass article.

After the initial crack branching occurs, the continued release of tensile energy acts to accelerate the propagation of the two new cracks until they, in turn, also reach the terminal velocity. At this point, each crack will bifurcate into two new cracks, i.e., for a total of four cracks. This process continues, with each new crack accelerating due to the release of stored tensile energy and subsequently bifurcating upon reaching terminal velocity. The final fragmentation pattern of the broken glass depends on the amount of stored tensile energy and the total fracture surface area, i.e., the thickness of the glass article. Stress profiles with high values of CT lead to a faster release rate of the stored tensile energy, and therefore a faster acceleration of each crack. In this situation, each crack reaches its terminal velocity after a short propagation distance. Ultimately, this causes the glass to fracture into a large number of small fragments, termed "frangible fracture." The quintessential example of frangibility occurs in the Prince Rupert's drop, which, upon fracture, disintegrates into tiny fragments of powdered glass due to the very high amount of stored tensile energy being released.[97]

Owing to the catastrophic nature of failure in frangible glasses, it is desirable for many glass products to stay below the frangibility limit of CT. However, there are also applications in which frangible fracture is a desired design criterion, e.g., side and backlite automotive glazing or single-sheet safety glasses, which are tailored for human safety to avoid large, sharp-cornered glass fragments. Thinner glasses have a lower threshold for frangibility compared to thicker glasses, i.e., the amount of CT required to experience frangibility is lower for thinner glass articles compared to thicker glass articles.[98] This is because a thinner glass has a lower fracture energy for the same crack distance (due to the lower crack surface area for an equivalent propagation distance). The lower frangibility limit of thin glasses places a tighter constraint on the amount of compressive stress that can be safely installed in them. This is a particular concern, e.g., for foldable electronic devices having ultrathin chemically strengthened cover glass (see Section 4).

To determine the frangibility limit of a given glass, samples must be prepared with stress profiles that yield CT values both above and below the frangibility limit. These samples must then be fractured in a controlled fashion so that only the minimal amount of force is applied to introduce a crack that barely penetrates through the zero-crossing point of stress. In this manner, the resulting fragmentation pattern depends only on the release of stored tensile energy from the glass and not on excess energy applied from the external impact.[99] This controlled crack initiation can be applied, e.g., by dropping a rod with a hard indenter tip from a known height. We note that the minimum number of fragments required for a sample to be declared as "frangible" is subjective and depends on the size and geometry of the sample.

High-speed cameras are especially effective tools for understanding the dynamics of fracture in frangible glass specimens.[100] Given a terminal velocity of ≈2 km s^{-1}, a camera with a frame rate of several $\approx 10^5$ fps is required to observe the sequence of crack bifurcation processes. **Figure 6** shows a sequence of frames of a high-speed video for a thermally strengthened glass sample with a CT value above the frangibility limit. With such video data, the statistics of crack propagation behavior can be obtained, viz., the distribution of crack lengths, velocities, bifurcation angles, etc. For example, for sufficiently high values of CT, crack trifurcation events can occur to further accelerate the release of stored tensile energy.[100] Similar high-speed observations have been applied to study the highly frangible behavior of Prince Rupert's drops[101] or crack front propagation in chemically strengthened glass in various ring-on-ring loading configurations.[102]

Despite recent progress, several challenges still exist with respect to glass frangibility, including understanding the transition from crack bifurcation to trifurcation at high stresses

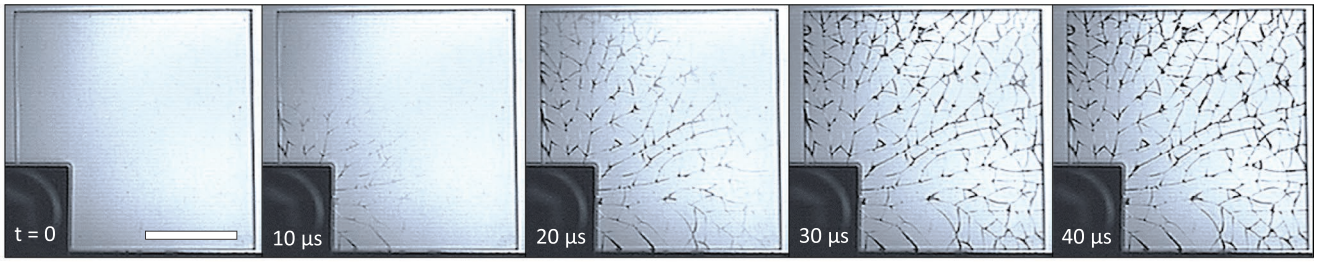

Figure 6. Video frame sequence of a fracture event observed in a thermally strengthened borosilicate glass sheet of 3.3 mm thickness. Collected in diffuse transmission mode at a rate of 10^5 fps. The scale bar is 20 mm.

and clarifying the role of tailored stress profiles in governing the shapes of the resulting fragments, for example, as strengthened via multistep ion exchange processes, by extreme thermal quenching, or by a superposition of thermal and chemical tempering. Another question concerns the role of embedded secondary phases in modifying the crack branching behavior, for example, in glass ceramics, glass-like composites, or phase-separated glasses (see Section 8). While high-speed cameras are powerful tools for characterizing fracture dynamics, obtaining sufficiently high image rate and, at the same time, image resolution to allow for statistically relevant kinetic analyses remains a further challenge.

6. Dynamic Fracture and Intrinsic Length Scales

The fracture toughness of glasses, quantified either by a critical stress intensity factor or by the fracture energy Γ, provides a measure for the critical conditions for the initiation of crack propagation in the presence of notch defects. While being of prime importance, it offers very limited information about the subsequent evolution of the propagating crack, whose dynamics may ultimately lead to the actual catastrophic failure. The propagation phase of crack dynamics—as opposed to the nucleation and initiation phases—which in brittle materials is associated with high propagation velocities v (of the order of the elastic wave speeds), is the main focus of the field of dynamic fracture.[103,104]

The conventional starting point for addressing dynamic fracture in brittle materials is the linear elastic fracture mechanics (LEFM) theory.[103,104] Within this framework, the deformation is assumed to be linear elastic to a very good approximation, except for a small region near the crack edge, where nonlinear and dissipative processes take place. The intrinsic material length scales associated with this near-edge region are assumed to be negligibly small compared to extrinsic length scales (e.g., crack length and the geometric dimensions of the sample) and hence to play no role in fracture dynamics. While it is clear that nonlinear and dissipative length scales are essential for understanding the toughness of glasses, the effect of such intrinsic material length scales is implicitly embedded in the framework of LEFM in the fracture energy Γ, but otherwise they do not appear in the theory.

Recent progress in understanding dynamic fracture of amorphous materials has revealed that in fact intrinsic material length scales may have profound implications for crack propagation, especially at high propagation velocities.[105–114] The effects of such intrinsic material length scales have been shown to be most pronounced in the context of dynamic fracture instabilities, i.e., in situations where dynamic cracks undergo spontaneous symmetry breaking, which remain poorly understood in general.[110,115] An example of such a symmetry-breaking instability, observed in thin brittle gels,[116] is shown in **Figure 7**a. A straight tensile (mode I) crack undergoes a transition to an oscillatory crack upon surpassing a very high propagation velocity (approximately 90% of the Rayleigh wave speed).[116] Moreover, and most importantly, the wavelength of oscillations has been shown to be independent of the dimensions of the sample, i.e., it is an intrinsic length scale missing from LEFM.

The oscillatory instability has been quantitatively explained based on the weakly nonlinear fracture mechanics (WNFM) theory,[106] which extends LEFM to account for leading order nonlinear elastic corrections near the propagating crack edge. This theory gives rise to a new intrinsic material length scale ℓ, which emerges from the competition between linear and nonlinear elastic near-edge deformation, scaling as $\ell \sim \Gamma(v)/\mu$.[106,107] Here, $\Gamma(v)$ is the velocity-dependent fracture energy, a generalization of the fracture energy Γ for dynamic fracture, and μ is the shear modulus (representing the magnitude of the elastic moduli).

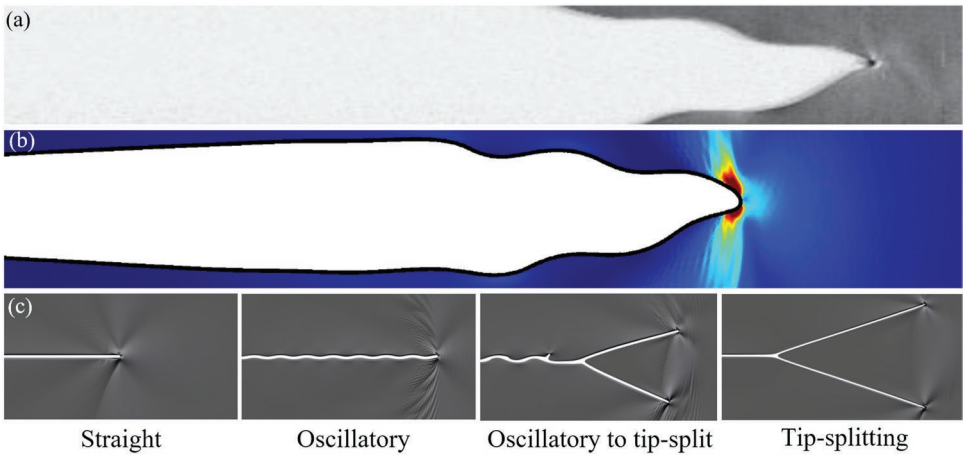

Figure 7. a) Experimental snapshot of the high-velocity oscillatory instability in quasi-2D dynamic fracture, observed in thin brittle gels.[112] The crack propagation velocity is ≈90% of the Rayleigh wave-speed and the oscillation wavelength here is on a mm scale, see details in ref. [112] b) The corresponding theoretical prediction based on large-scale phase-field fracture simulations,[112] where the intrinsic nonlinear length ℓ is incorporated (see text for details). The color code represents the magnitude of the elastic strain energy (in the unit of μ). The theoretical predictions have been shown to be in quantitative agreement with experiments, where ℓ controls the wavelength of oscillation. c) A sequence of dynamic fracture instabilities predicted in thin brittle samples.[114] From left to right, shown are a straight crack (left most panel), an oscillatory crack (second panel), an oscillatory crack, where subsequent frustrated and successful tip-splitting take place (third panel), and a direct transition from a straight crack to a tip-split crack (rightmost panel), see additional details in ref. [114] a,b) Reproduced with permission.[112] Copyright 2017, Springer Nature. c) Reproduced with permission.[114] Copyright 2021, Elsevier.

Incorporating these ideas into a phase-field fracture approach and performing large-scale numerical simulations have revealed an oscillatory instability, as shown in Figure 7b.[112] The instability onset and its subsequent properties have been shown to quantitatively agree with experiments on various brittle gels, and in particular, it has been shown that the intrinsic nonlinear elastic length ℓ determines the wavelength of the oscillations.[112,113]

Very recently,[114] it has been shown that in materials in which near crack edge elastic nonlinearity is negligibly small, i.e., in the limit $\ell \to 0$, the oscillatory instability persists, but with a wavelength that is controlled by another intrinsic length scale that is missing from LEFM, the near edge dissipation length ξ (e.g., the plastic zone size).[112,114] The transition from straight to oscillatory cracks at high propagation velocities, shown in Figure 7c (two leftmost panels), is not the only instability discovered in thin, quasi-2D amorphous materials. In fact, it has been predicted that upon increasing the driving force for fracture, oscillatory cracks can undergo frustrated and successful tip-splitting, which is yet another symmetry-breaking instability.[113] This prediction, demonstrated in Figure 7c (third panel from left), has been subsequently confirmed experimentally.[113] Further increasing the driving force for fracture may result in a direct transition from a straight crack to a symmetrically tip-split crack, as demonstrated in Figure 7c (rightmost panel). When thick samples are considered, i.e., when fracture is fully 3D as in most real-life situations, other remarkable symmetry-breaking instabilities such as the microbranching one have been observed in a variety of glassy materials.[110,115,117] Understanding these 3D dynamic fracture instabilities, and their possible relations to intrinsic material length scales, remains a major open challenge. Finally, the intrinsic material length scales ξ and ℓ (and their generalizations) have been shown to play major roles in the fracture of soft materials that can undergo large elastic deformation prior to failure.[118] Meeting the challenge of better understanding dynamic fracture in three dimensions, which is also directly relevant for the discussion in the previous Section 5, is required for practical glass development, and in particular for tailoring glass properties.

7. Computational Studies of Glass Mechanical Behavior

In this section, we will focus on challenges and trends concerning silicate and, for their technological importance, borosilicate glasses. We note that many of the findings and efforts reported in the previous Sections 2, 3, and 6 similarly rely on computational simulations. For a more comprehensive overview of computer simulation techniques applied in glass science, see refs. [119–121].

7.1. Molecular Dynamics Simulations

While experimental measurements are necessary to determine the mechanical performance of glass, MD simulations can provide complementary insights regarding the atomic-scale response of a glass to mechanical stress.[122] MD simulations follow the trajectories of each atom in a system by integrating Newton's second law of motion. Such simulations are limited in length and time scales as well as accuracy by the available computing power.[123] The accuracy depends on the quality of the interatomic force fields, which describe the interactions between atoms. For example, chemical accuracy is obtained on the coupled cluster with singles and doubles level, however, in this case, the accessible model size is currently limited to only a few atoms.[27] As noted in Section 3, comparably small computer glass samples (e.g., a few thousand atoms) are beneficial in the study of glassy vibrational excitations, as they avoid hybridization/mixing with low-frequency phonons.[67,68]

Recent larger-scale simulations have enabled the study of the atomic scale response of glass to various loading conditions, including indentation, using systems of up to 1.8 million atoms.[124] The primary difficulty of such models is to integrate high accuracy and chemical complexity with system size so as to approach the pertinent length scales of mechanical response. For example, borosilicate glasses have proved particularly challenging for MD simulations due to the boron anomaly, i.e., the conversion of boron from trigonal to tetrahedral coordination in the presence of modifier cations. Recently, two new sets of interatomic force fields have been developed by Wang et al.[125] and by Deng and Du[126] for borosilicate glasses, both of which accurately capture the boron anomaly across a wide range of compositions. Since boron can also change coordination in response to stress, the ability to capture the boron coordination change with MD simulations is critical for understanding the mechanical response of these glasses.[51,127,128] In particular, the presence of a high concentration of trigonally coordinated boron provides higher resistance of the glass to defect formation upon mechanical stimulation (e.g., indentation or scratching). The improved damage resistance of these glasses is due to their ability to dissipate energy via plastic deformation prior to crack initiation.[129,130]

A series of recent studies[131–134] applied MD simulations using both the Wang et al.[125] and Deng and Du[126] force fields to study the mechanical response of two industrial borosilicate glasses, SCHOTT Borofloat33 (Boro33) and SCHOTT N-BK7 (N-BK7), under different loading conditions to obtain an atomic-scale understanding of the various deformation mechanisms experienced by these glasses. MD simulations of the cold-compressed glasses revealed that trigonally coordinated boron facilitates densification in response to applied pressure, while high-coordinated network formers are mostly unaffected.[131] Investigations of the shear deformation behavior under different pressures revealed that the addition of alkali ions lowers the yield stress and changes the pressure dependence of the shear modulus.[133] A shear-induced densification mechanism was also observed in both Boro33 and N-BK7 systems, which is attributed to changes in both the oxygen-centered bond angle and the coordination number of boron. At higher pressures, there is also an increase in the population of five-coordinated silicon atoms. The atomic shear stresses calculated from the MD simulations indicate that boron species can relax mechanical stresses more readily under pressurized shear compared to other constituents of the glass. This is especially true in Boro33, owing to its higher concentration of trigonally coordinated boron compared to N-BK7. In the latter case,

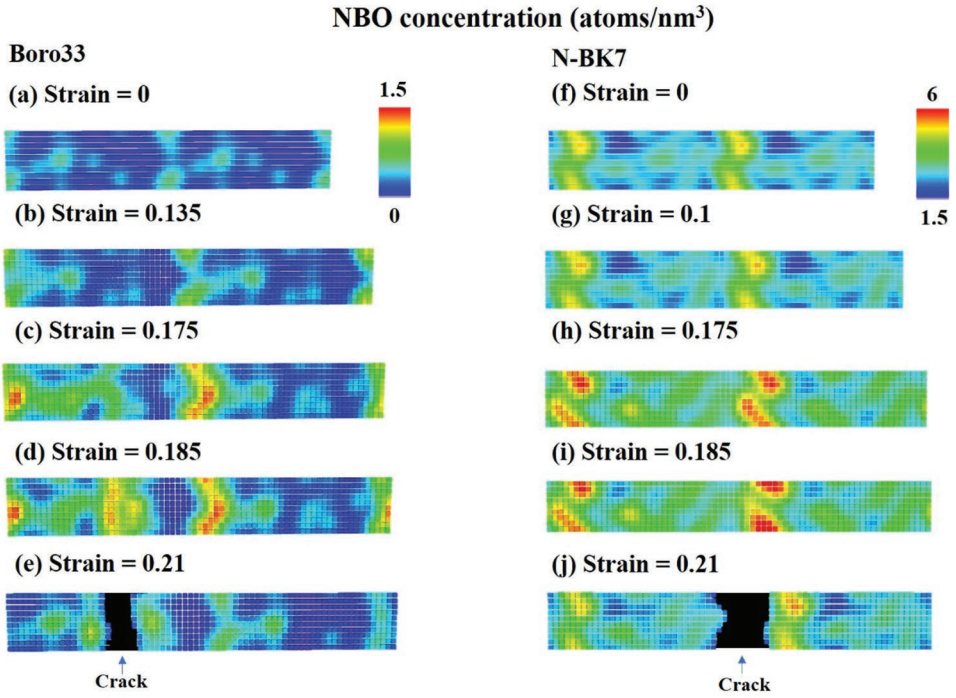

Figure 8. MD-simulated evolution of NBO distributions (atoms nm^{-3}) during uniaxial tension tests for Boro33 and N-BK7 borosilicate glasses. The samples fractured at the strain of 0.21. Reproduced with permission.[134] Copyright 2020, John Wiley & Sons.

plastic deformation is also facilitated by alkali-rich regions in the glass.

The plastic response of these borosilicate glasses under uniaxial tension was also investigated, and for both Boro33 and N-BK7, it is found to be governed by an irreversible bond-switching mechanism enabled by the production of non-bridging oxygen (NBO) during the application of uniaxial tension.[134] The B^4—O—Si linkages are more effective at creating NBOs compared to Si—O—Si linkages in borosilicate glasses when the systems are exposed to uniaxial tension. The presence of NBOs also reduces the force required for breaking the B^4—O bond in B^4—O—Si units, which in turn lowers the yield strength of the glass. **Figure 8** shows the calculated evolution of the NBO population in Boro33 and N-BK7 glasses during the uniaxial tension simulations. Panels (a) and (f) of the figure show that the initial NBO distributions are heterogeneous in both glasses. This observed nano-segregation is consistent with Greaves' modified random network (MRN) model of silicate glass structure.[135] Figure 8 also shows that when uniaxial tension is applied, high-NBO regions develop. Fracture ultimately occurs in the weakest cross-section of the sample, viz., containing a high local concentration of NBOs.

MD simulations of the response of sodium borosilicate glasses to nanoindentation have shown that a greater amount of densification is observed in glasses that have initially lower network connectivity, i.e., a higher fraction of trigonally coordinated boron.[136,137] The coordination numbers of boron and sodium both increase under the indenter, whereas the coordination number of silicon is unchanged. These simulations thus further emphasize the important role of threefold-coordinated boron in enabling plastic deformation under an applied load.

7.2. Finite Element and Peridynamics Simulation Methods

MD simulations do not traditionally allow the study of stress distribution and fracture patterns on scales beyond the nanoscale due to the high computational cost associated with these methods. To overcome this difficulty, experimental techniques are available.[138,139] On the other hand, the finite element method (FEM) and peridynamics simulations have been widely successful in studying 3D stress and strain distributions in situ on micro- and macrostructural scales. Furthermore, other methods, such as the phase-field fracture approach (on which some results discussed in Section 6 are based[113–115]), have been developed and extensively used in glass science. A disadvantage of FEM is that it cannot handle stress discontinuities, for example, such as occurring in the vicinity of crack tips. This issue is solved with the peridynamics technique. Peridynamics involves a nonlocal reformulation where the partial differential equations of solid mechanics are replaced with integral equations.[140]

FEM calculations rely on input from material properties and the selection of a mesh refinement.[141] A very active research field within FEM simulations on glasses is the modeling of indentation-induced stress and strain fields with accurate constitutive laws. Various models, including von Mises, Mohr-Coulomb, and Drucker-Prager criteria, have been used to numerically analyze load-displacement curves, elastic recovery, deformation mechanism (densification, pile-ups), etc.[142–145] Some of these predictions can be validated experimentally. Also glass fracture has been studied, for example, based on the introduction of cohesive element planes to the finite element mesh[146] and the use of discrete element modeling.[147] These developments now make it possible to calculate accurate stress and strain fields, at least in some selected silicate glasses for which sufficient

material information is available to construct constitutive laws. Such simulations have very recently helped to understand glass hardness and the pertinent deformation routes.[148]

To account for stress discontinuities, and further to allow for an improved description of crack branching as relevant for frangibility (Sections 5 and 6), peridynamics simulations are an attractive alternative to FEM.[149] Similar to FEM, they require input from material properties, but do not involve a mesh and are, therefore, scale invariant. For example, peridynamics simulation has been used to study dynamic crack propagation,[150] impact damage,[151] and the indentation response of glasses.[152] For example, the self-affine growth of cracks in glass upon impact loading has been shown to lead to a power-law dependence between the total damage and the fracture energy of the glass plate.[151] Peridynamics simulations can offer good agreement with experimental load–displacement curves and the derived indentation stiffness and hardness for a soda-lime silicate glass, despite not capturing shear flow and permanent densification.[152] **Figure 9** shows the calculated stress distribution around an indenter, with the butterfly-like shape matching the elastic stress distribution observed in silicon by micro-Raman mapping.[153] Overall, these studies demonstrate the suitability of peridynamics in support of experiments for gaining new insights into the fracture behavior of glasses upon impact and sharp-contact loading. Alternatively, phase-field simulations can be used to model the nucleation, growth, and bifurcation of cracks,[154] such as shown in Figure 7. Being based on Griffith's fundamental work, this method involves the minimization of an energy functional, with various formulations being proposed.[155] For example, phase-field simulations have recently been used to study crack patterns in glass laminates.[156]

8. Emerging Glass Types with Optical Transparency and Tailored Mechanics

8.1. Oxide Glasses from the Bottom-Up

In recent years, the design of new oxide glass compositions with improved mechanical properties has shifted its focus toward bottom-up approaches,[2] as illustrated in **Figure 10**. That is, by utilizing knowledge of the deformation mechanism of oxide glasses under high local stress, and by appropriately tailoring microstructures, glass materials with improved resistance to crack (defect) formation and growth have been discovered. Where early attempts to produce crack-resistant oxide glasses focused primarily on maximizing free volume,[54] it has become clear that in depth tuning of glass chemistry is crucial for further progress. For example, µm-sized binary aluminosilicate glasses made by aerodynamic levitation show in principle that the cracking resistance can be increased even with an increase in atomic packing density.[157] To obtain hard and stiff glasses, the focus has traditionally been on designing networks with high atomic packing density and high dissociation energy of the oxide components.[158] For example, this has been achieved in glasses with high content of Al_2O_3 and high field strength cations.[159,160]

Recently, the mixing of five or more oxide components (to achieve so-called "high-entropy" materials) has also been proposed for glasses, demonstrating the containerless synthesis of a $(La,Sm,Gd)_2O_3$–Y_2O_3–TiO_2–ZrO_2–Al_2O_3 glass with high hardness (>12 GPa) and high Young's modulus (>170 GPa).[161] For such ultrastiff glasses (which usually rely on heavy loading of rare earth oxides), it is challenging is to adapt their composition in such a way that larger glass objects can be produced. It typically means that the number of chemical components must be increased, for example, such as in the popular alkaline earth aluminosilicate glasses, which may accommodate high amounts of rare earth doping and still be meltable by regular laboratory techniques.[162] Here, the field of optical glasses and, in particular, high-index or magneto-optical materials provides a rich resource of glass chemical knowledge, which can be transferred to the study of mechanical performance (e.g., see refs. [163,164]). Given the expected chemical complexity of these glasses, this area offers a playground for combinatorial methods and approaches supported by machine learning.

Glasses with high contents of trigonal boron and tetrahedral aluminum, which are prone to undergo an increase in coordination number even under modest stress, enable facile stress dissipation and thus high resistance to sharp contact

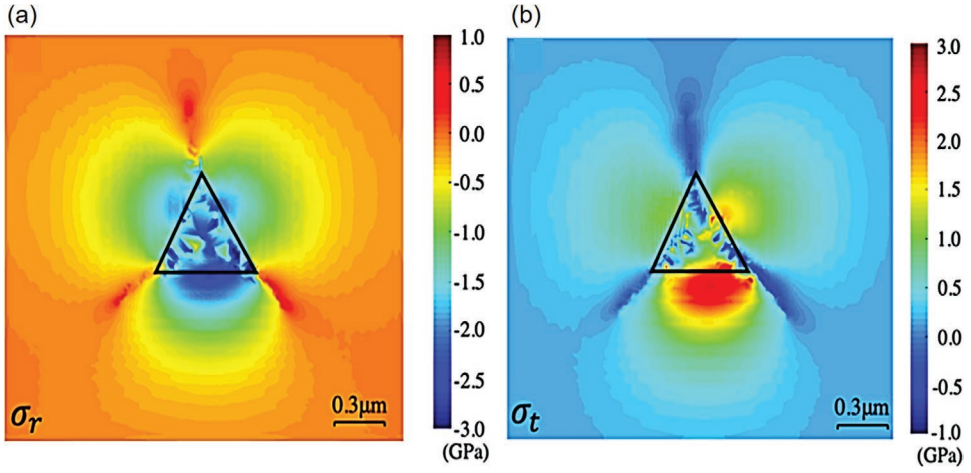

Figure 9. Peridynamics calculated a) radial and b) tangential stress distribution in the plane along which the indenter tip enters in contact with the soda-lime silicate glass. The resulting stress is localized at the vicinity of the indenter (black triangle indicates the extent of the projected contact area with the indenter). Reproduced with permission.[152] Copyright 2021, John Wiley & Sons.

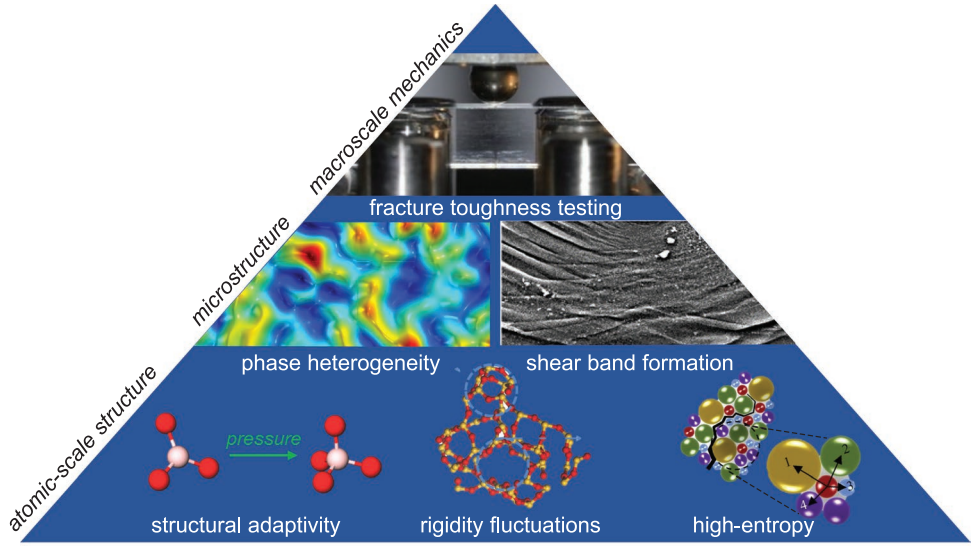

Figure 10. Bottom-up design of oxide glasses with improved mechanical properties. Examples of design strategies from the atomic- and microstructural scales are highlighted, resulting in improved macroscale mechanics. The individual figure panels are reproduced under the terms of a Creative Commons Attribution License (CC BY 4.0).[81] Copyright 2018, The Authors, published by Wiley-VCH, Reproduced with permission.[167] Copyright 2017, American Chemical Society), Reproduced with permission.[170] Copyright 2018, Elsevier and Reproduced with permission.[207] Copyright 2018, Elsevier), and Reproduced with permission under the terms of a Creative Commons Attribution License (CC BY-NC-ND 4.0).[161] Copyright 2021, The Authors, published by AAAS.

crack initiation,[165,166] as discussed in Section 7. This phenomenon, which is especially pronounced in aluminoborate glasses with low field strength modifiers, has been referred to as self-adaptivity of the glass network.[167] High crack initiation resistance has also been achieved in so-called intermediate calcium aluminoborosilicate glasses, which exhibit both densification and shear flow deformation behavior upon indentation. By tuning the boron-to-silicon ratio in defect-resistant borosilicate glasses,[168,169] it is possible to enable shear-banding; glasses with high shear band density are found to be less prone to the formation of subsurface shear faults.[170] Following up on the study of vibrational disorder (Section 3), nanoscale fluctuations in the network rigidity have been found to mediate the experimental deformation process, similar to granular media with pronounced intergranular cohesion.[81] The statistics of such fluctuations might offer a further criterion for property tailoring,[78] however, the exact nature of heterogeneity remains unknown for chemically more complex glass formulations. Lateral indentation testing (scratching) experiments offer a practical view and understanding in this direction, with a focus on the role of structural cohesion on scratch hardness[171–173] and deformation modes.[174,175]

Beyond hardness, stiffness and indentation response, designing tough oxide glasses continues to be a major challenge. The fracture toughness of most oxide glasses, as measured using self-consistent methods, remains below 1 MPa $m^{0.5}$. Glass fracture toughness can be estimated from the interatomic bond strengths and the bond concentration along a fracture surface, assuming the absence of plasticity.[176,177] Structural densification has found to be a promising route, as it can increase rigidity and crack tip blunting, leading to stress relaxation.[178] As shown in simulations, tuning of cooling rates (see Section 3) or pressure can also be used to induce a brittle-to-ductile transition,[179] as can consolidated glassy nanoparticles in silica.[180] The latter leads to formation of fivefold coordinated silicon, which has a higher propensity to carry out local shear deformation than four-fold coordinated silicon, leading to the observed nanoscale tensile ductility.[180] In experiments, high-temperature densification of a bulk aluminoborate can lead to a toughness of 1.4 MPa $m^{0.5}$, as densification enhances the bond switching dynamics.[181] The ability of glasses to deform plastically to an extent far beyond the predictions of the classical cohesive zone model[103]—on nanometer scale—is often termed nanoductility. It has been observed experimentally in glassy silica,[182–184] but also, e.g., in flaw-free thin films of amorphous alumina at high strain rate,[45] as already discussed in Section 2.

Besides compositional adjustments and established post-processing methodology,[21] other techniques are presently being explored to improve the mechanical properties of transparent oxide glasses, including nanoscale phase-separation, partial crystallization to produce glass-ceramics, and (surface) hydration. Liquid-liquid phase separation has been proposed as a means to improve fracture toughness, but so far, experimental demonstrations have been relatively limited and mostly restricted to indentation studies.[185,186] As shown by computational simulation, the presence of a secondary phase in glasses undergoing phase separation can impede crack propagation through crack arrest, crack deflection, and diversion, which can increase the fracture toughness.[187,188] Using peridynamics, the extent of toughening was found to be due to a balance between propensity for crack deflections, effective cohesion of the phase-separated glass, existence of plastic energy dissipation, and roughness of the crack surface.[187] Such studies are—in principle—related to glass ceramic design, which leads to a similar two- or three-phase materials. The mechanical properties of glass ceramics, typically prepared through a two-step heat

treatment to induce nucleation and crystal growth, have been explored through both experiments and simulations, reporting improvements in both strength and fracture toughness.[189,190]

Due to the breadth of the topic and a somewhat different application focus, however, we will not discuss glass ceramics at this point; a recent overview is provided in ref. [191]. Noteworthy, glass ceramics have recently been introduced to replace pure glass covers in mobile phone devices.[192] For both glass ceramics and phase-separated glasses, an important issue for most applications is to retain transparency, requiring that the size of the formed structures is small relative to the wavelength of visible light, and that the refractive indices of the involved phases are similar and, preferentially, isotropic. Such control is possible, for example, as shown in the case of phase separation in calcium aluminosilicate glasses, where the domain size, morphology, and phase distribution can be finely tuned.[193,194] Simulations have shown that soft, yet tough nanoinclusions may provide for the largest toughening effect,[187] what now requires experimental verification and the demonstration of retained optical transparency. Very similar design considerations have to be made in the context of transparent hybrid and composite structures, as will be discussed later in this section.

A different route to glasses with enhanced surface defect resistance focuses on surface hydration.[195] When oxide glasses are exposed to water (at variable temperature and/or pressure), their surface is hydrated. This is accompanied by a practical improvement on performance in crack initiation studies. The strengthening mechanism remains to be fully understood, but could involve crack tip shielding,[196] stress relaxation,[197] and/or compressive stress generation.[198] The effect has been found in various glass compositions, from a very soluble cesium aluminoborate glass, for which hydration (which renders the glass surface into a gel-like layer) can lead to record-high crack resistance,[199] to more durable silicate-based glasses treated at higher humidity and/or temperature, as reported in recent patent applications.[198,200] Of potentially high interest, glasses that contain water not only on their surface but also in their bulk have been demonstrated to not only perform well in defect initiation studies, but to also exhibit highly tunable elastic properties.[33,34]

Progress on the area of oxide glass development has thus far been based on knowledge of glass chemistry and structure; the next level will be to implement this knowledge with high-throughput methodologies, for example, using machine learning (ML). For oxide glasses, this involves automated literature screening to mine model training and validation data from text, tables, and figures.[201] ML models, mostly based on neural networks, have been developed to predict mechanical properties such as hardness and elastic modulus;[202] however, improved predictions will require physical descriptors instead of simple glass composition data. The search for such descriptors can be guided by classification-based ML. For example, while structural descriptors such as local density, free volume, or bond localization, and orientation have already been linked to flow defects, they are insufficient to fully predict glass fracture.[203] Alternatively, a nonintuitive structural metric termed "softness" was found to be strongly correlated with the dynamics of specific atoms based on their local structural environments,[204] and has been successfully linked with creep dynamics and yielding behavior of disordered materials.[205,58] Very recently, it has also been shown that this metric can be trained from the spontaneous dynamics of glass under zero strain, and then used to predict the glass' fracture propensity under strain.[206] In particular, rapid crack propagation occurs upon the local accumulation of high-softness regions. As these studies suggest, advances in new oxide glass composition design are expected to come from coupling knowledge of nanoscale deformation processes with high-throughput ML methods. It remains to be explored how such understanding can be coupled to parallel physical insight as to the nature of elastic disorder (see Section 3).

8.2. Glasses from Organic–Inorganic Hybrids

Engineering oxide glasses have numerous applications as discussed in this review, mostly building on their optical transparency, mechanical stiffness, and chemical inertness, but they suffer from poor impact and fracture resistance. Glass strength can be improved through thermal or chemical strengthening, but these treatments do not significantly increase fracture toughness (see Section 2) and can lead to frangible fracture, especially for thin glasses (see Section 5). Compositional tuning of oxide glasses also has limitations, since around 3/5 of the atoms are typically oxygens, while conventional metallic glasses are not transparent and chalcogenide glasses are even less tough than oxides.[177] To overcome these limitations, the possibility to tune the micro- and nanoscale structures of disordered materials by combining organic and inorganic constituents has been explored, as these hybrids offer enormous chemical versatility due to their exchangeable building units.

An important family of hybrid materials involves conetworks of organic and inorganic components with molecular-scale interactions and covalent links that make them indistinguishable at the nanoscale and beyond. They can thus be different from the transparent composites and bioinspired materials covered in the following paragraph, and avoid any poor interface bonding.[208] Such amorphous hybrid materials are usually made by sol-gel processing, in which a solution (sol) containing the inorganic precursors undergoes crosslinking reactions at room temperature to form a gel.[209] The gel is a wet inorganic network (typically of covalently bonded silica), which can be dried and heated to form an amorphous solid. Hybrids are synthesized by introducing an organic polymer early in the sol-gel process to enable the inorganic network to form around the polymer molecules.

To create interpenetrating networks that interact at the molecular level, a coupling agent is needed to act as a bridge between the two components.[210] The resulting sol–gel hybrid amorphous material acts as a single phase with congruent physiochemical behavior, and it can be used directly as an ink for 3D printing without the need for additional binders. Jones et al. made a triple network hybrid sol-gel material (**Figure 11**a), showing elastomeric "bouncy" behavior and ability to self-heal within seconds after fracture without external stimulus, yet with an ability to biodegrade.[211] Varying the organic component, e.g., by using tetrahydropyran with an additional C atom instead of tetrahydrofuran as the monomer, enables a structural control of the mechanical flexibility and self-healing propensity.[212]

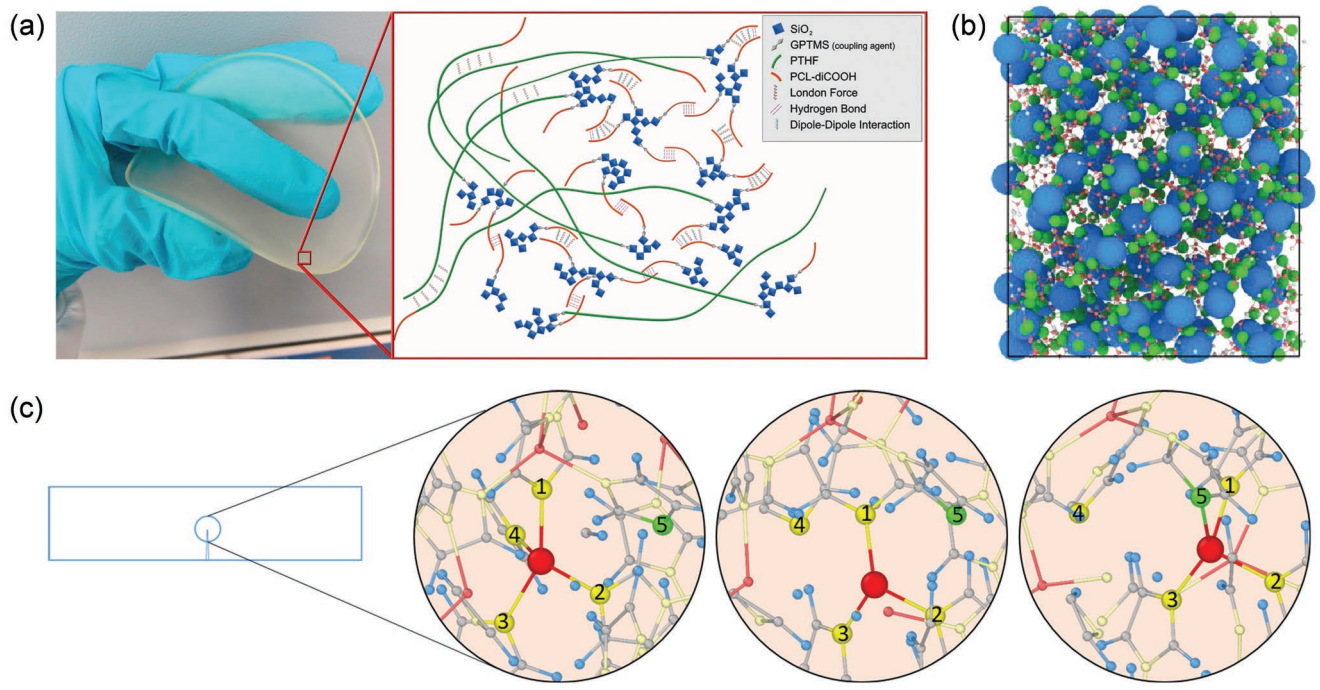

Figure 11. Hybrid noncrystalline materials with tailored nanostructures to control their mechanical deformation behavior. a) Bending and microstructure of silica/poly(tetrahydrofuran)/poly(e-caprolactone) hybrid material. Reproduced with permission.[231] Copyright 2021, Elsevier. b) Simulated atomic-scale structure of ZIF-62 ($Zn(Im)_{1.75}(bIm)_{0.25}$) melt-quenched glass. Reproduced with permission.[232] Copyright 2020, American Chemical Society. c) Simulated bond switching mechanism in ZIF-62 glass, showing how the central Zn atom (in red) transitions from fourfold to threefold and back to fourfold coordination with N upon increasing strain (ε) from $\varepsilon = 0$ (left) to $\varepsilon = 0.09$ (middle) and $\varepsilon = 0.42$ (right). Adapted with permission.[226] Copyright 2021, Royal Society of Chemistry.

Likewise, mixing of silica with titania as the inorganic component has been shown to improve the compressive failure strain and strength.[213] With the proper tuning of their mechanical properties, such hybrids are attractive bioactive materials, e.g., for cartilage regeneration.[214]

Recently, metal organic framework (MOF) and coordination polymer (CP) glasses have emerged as further noncrystalline, hybrid material families.[215] MOF/CP crystals are porous materials formed from inorganic nodes connected to organic ligands, but they are not available in bulk pieces. As a concept, this can be overcome by melting and quenching them to form MOF/CP glasses. However, despite the fact that around 10^5 variations of MOF and CP crystals with diverse structural motifs have been reported, only a small fraction of these have been turned into glasses. Unlike the challenge in metallic systems, where the need for a high critical cooling rate is the main limitation for glass formation, in MOF/CP systems, the limitation is the access to a stable liquid state. That is, many of the porous crystals thermally decompose before they melt.[216] To enable glass formation, the strategy could be to lower the melting temperature, e.g., by using crystals with large entropy difference to the liquid state,[217] by incorporating an ionic liquid into the porous interior,[218] or increasing the temperature of thermal decomposition. The latter has been a very successful strategy in terms of making zeolitic imidazolate framework (ZIF) glasses with thermally stable ligands (Figure 11b).[219,220] For example, ZIF-76-mbIm glass ($Zn(Im)_{1.33}(mbIm)_{0.67}$, where Im = imidazolate and mbIm = 5-methylbenzimidazolate) features pronounced nanoscale porosity,[221] while it has been shown that ZIF-62 glass ($Zn(Im)_{1.75}(bIm)_{0.25}$, where bIm = benzimidazolate) avoids the formation of intercrystalline defects in membranes, showing enhanced molecular sieving ability compared to the crystalline membrane.[13] Understanding the microscopic deformation and fracture mechanisms of these nascent materials will be of high importance for their postprocessing and applications.

While we are not aware of any mechanics studies on CP glasses, most studies on mechanical properties of MOF glasses have so far focused on ZIF-62, due to its ultrahigh glass-forming ability and the possibility to fabricate comparably large (>10 mm) bubble-free samples suitable for mechanical testing.[222,223] Fracture toughness (K_{Ic}) testing, using the single-edge precracked beam method, revealed that this glass features a low K_{Ic} of around 0.1 MPa $m^{0.5}$, which is even lower than that of traditional oxide and chalcogenide glasses.[224] Compoundation of ZIF-type glasses with inorganic glasses was considered as a potential means to further improve the mechanical performance of this new class of materials.[225] Thereby, the inorganic component was chosen so as to match the melting range of the ZIF, enabling comelting.

Although the ZIF glasses feature nanoscale ductility via bond switching[226] and the relatively high Poisson's ratio (≈0.34) might indicate a more ductile fracture behavior,[82] the low toughness is ascribed to the preferential breakage of the weak Zn—N coordination bonds (Figure 11c). Indeed, the coordination bonds control a wide range of their mechanical behavior

and have also been associated with indentation-induced shear bands, which are typically not seen in other network glasses with a fully polymerized structure.[227] Nanoindentation studies have shown that the elastic modulus of different ZIF glasses is positively correlated with the pycnometric density[228] and hardness.[223] Moreover, their strain-rate sensitivity was found to be similar to that of glassy polymers and Se-rich chalcogenide glasses.[223] However, to date, such interpretations remain tentative, given the difficulties of fabricating high-quality samples at statistically relevant scales, and furthermore, the presently unknown interplay of intrinsic and extrinsic effects.

As the most recent example of hybrid glasses, glassy materials derived from organic–inorganic perovskites have been reported.[229,230] For example, dicyanamide-based perovskite glasses have been discovered with Young's modulus of around 6–7 GPa, intermediate between typical values for organic and inorganic materials.[230]

Overall, these studies suggest that some improvement of hybrid glass mechanical properties may be needed depending on the application, but the chemical flexibility of both organic and inorganic building units should allow for this. Accessing "forbidden" glass states through high-pressure treatment or making composite materials are other promising routes for property tuning.[216]

8.3. Bioinspired Transparent Composites

In a final comment, we would like to turn to glass-like composites, which have been proposed as potential alternatives to glassy materials, combining the stiffness and scratch hardness of inorganic glasses with the impact resistance of plastic materials.[233,234] Research into these materials was originally driven by potential application in automotive glazing, where weight reduction and improved impact resistance were sought. Meanwhile, however, the potential fields of application have widened, although the major challenges remain: beyond simple matching of refractive indices, thermal and stress optical dissipation must be considered.[235] Furthermore, packing density and the relative fractions of the involved phases, interface mechanics and compatibility, and texture cannot be tailored sufficiently within the limits of conventional methods. On the other hand, natural biological materials have been an increasingly powerful inspiration for synthetic composites and, potentially, the design of glass-like materials with adapted mechanical performance. They use an array of strategies that can be grossly grouped into:[236] fibrous structures (tendons), helical structures resisting torsional loads (insect exoskeletons), gradients (human teeth), layered (mollusk shell), tubular-structures (mammalian horn and hoof), cellular pores (bones of birds), sutured materials (leatherback turtles), and overlapping plates (shark skin).

Despite the differences in these approaches, and moreover the diversity of species, there is one ubiquitous principle employed by all structural biological materials: their remarkable mechanics are possible due to their mixture of soft and hard phases.[237] To realize such a structured composite, biology typically utilizes a hierarchical structure, formed through a bottom-up self-assembly process. The soft component is usually a biopolymer protein, such as collagen, elastin, or keratin, while the hard component is typically an inorganic mineral, such as calcium carbonate, hydroxyapatite, or silica. When combined, the soft part imbues the material with strength and the ability to sustain a certain degree of plastic (ductile) deformation, while the hard part contributes stiffness and toughness.

Here, we will focus on nacre, the tough inner layer produced by mollusk shells, as an excellent example of a structural biomaterial (**Figure 12**); its design of geometry asymmetric phases can lead to remarkable mechanical properties of the composite structure in comparison with its building blocks. The mineral part (aragonite) forms about 95% of its volume, i.e., only a minor part of the volume is soft biopolymer (Figure 12d). Thus, although fragile mineral elements form a major part of nacre, the composite is 3000 times tougher than hard ceramic platelets[238] and it can undergo up to 1% of strain, which is remarkable compared to the ceramic building blocks.[239] Several mechanisms have been proposed to explain the enhanced performance of nacre under mechanical loads. One of which is related to the tough organic biopolymer between the tablets,[240] which resists shear movement of the tablets and often unfolds, contributing to energy dissipation.[241] Nanoasperities on the tablet surface[242,243] and bridges between the tablets[244,245] also provide key toughening mechanisms. Interlocking between the platelets due to their small waviness,[245,239] and the periodic tessellation structure[246–248] in particular, contribute to toughening. Understanding these mechanisms is critical for researchers to recreate the enhanced composite mechanics observed in nature.

The structure and performance of nacre have served as models for researchers in efforts to create bioinspired tough composites, with a principal challenge being the methodology of structuring the phases. Natural biological systems rely on self-assembly, and researchers have used similar approaches such as layer-by layer assembly, where a substrate is dipped sequentially into different solutions. This ensures that each immersion produces only one layer on the substrate,[249] thus requiring many immersions to reach an acceptable thickness.[250–258]

Freeze casting or ice templating employs a slurry of ceramic and water. The slurry is frozen from the bottom and the formation of lamellar ice crystals entraps the ceramic particles. Upon freeze-drying and water sublimation, a porous template of the ice structure remains. Then, after sintering of the ceramic phase, it is possible to infiltrate a second soft phase into the structure to fill the pores and mimic nacre layering.[259–261] The ceramic particle size, freezing rate, and ceramic concentration impact the microstructure,[262,263] as do additives such as glycerol, sucrose, sodium chloride, citric water, ethanol, and PVA,[264–266] by controlling the temperature gradient,[263,267–269] or external electric[270] and magnetic[271,272] fields. 3D printing is another important and popular technique which has been widely used, including stereolithography[273]), and fused deposition modeling.[274,275] Multimaterial 3D printers are capable of printing both soft and hard phases of the structure simultaneously, producing brick and mortar structures in a single step.[276,277]

While the vast majority of bioinspired composites have focused on optimizing mechanics, some of these have also

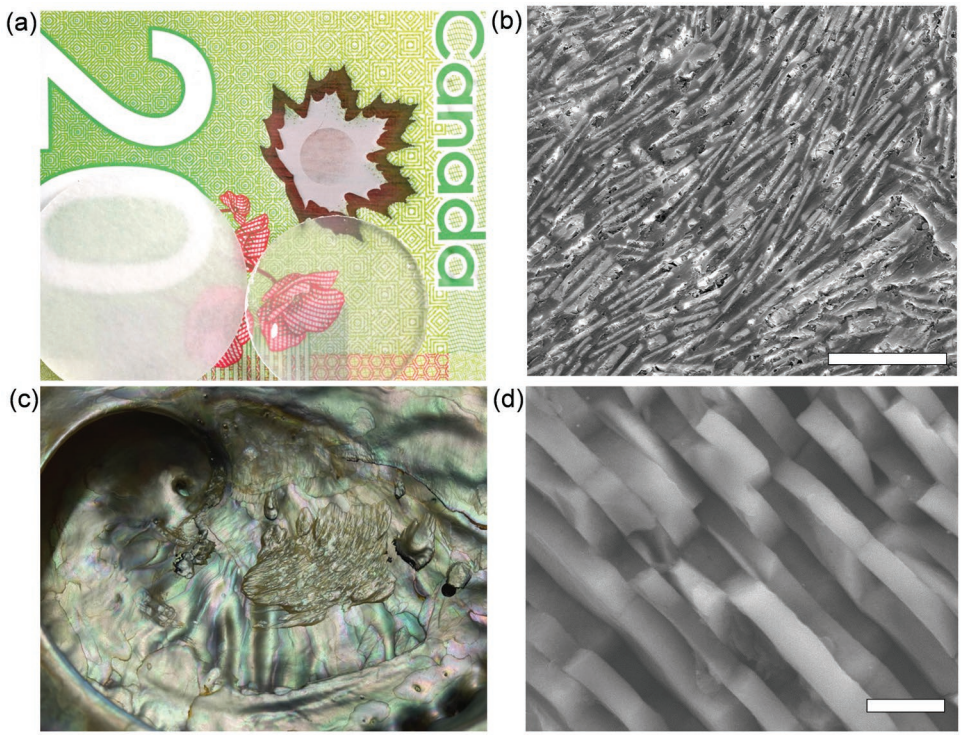

Figure 12. Nacreous composites for tough transparent glass. a) PMMA–glass composite with PMMA index matched to glass (top, transparent) or neat state (bottom, translucent). b) SEM microstructure of glass flakes connected in PMMA continuum. c) Natural nacre surface. d) SEM microstructure of well-ordered brick and mortar natural nacre structure. The scale bars in (b) and (d) are 20 µm and 3 µm, respectively.

endeavored to optimize composite transparency, as recently reviewed by Magrini et al.[278] Stronger transparent glasses have tremendous industrial and commercial value, and there has been a growing need for these in diverse markets. Many of the strengthening strategies result in optically and mechanically enhanced thin films.[254,255] Chemically strengthened glasses have been employed at large as they offer exceptional strength, however, chemical strengthening does not per se increase toughness.[21] Top-down methods, including laser-engraving interlocking 3D arrays in glass,[238] lamination of thin glasses with laser-engraved cross-ply,[279] and tablet-like architectures[238] have produced composites with increased fracture toughness and impact resistance, but reduced stiffness and strength. While stiffness and strength can be generally improved by decreasing the size of the tessellated patterns, this increases interfaces, decreasing transparency, and further hampers scalability.[280] A more scalable nacreous composite was created by infiltrating poly (methyl methacrylate) (PMMA) into a glass tablet scaffold, yielding a composite with superior fracture resistance. However, despite employing two transparent materials, the resulting composite is translucent rather than transparent.[278] This highlights a general trade-off challenge that bio-inspired glasses have suffered from between mechanics, transparency, and fabrication scalability.

Progress has continued with improved transparency in strong nacreous glasses, yet modest toughness.[281] It was recently shown that closely index matching the PMMA with the glass can markedly improve transparency (Figure 12a). Centrifuging the glass–PMMA mixture before the PMMA has been cured increases the glass volume fraction and induces a layered, ordered structure (Figure 12b). Together, these processes yield a leading nacre-like composite in terms of scalability, transparency, toughness, and strength that, unlike other glasses, can easily be cut and machined.[282] Nevertheless, current PMMA composite glasses still suffer from easy surface scratch damage due to the relatively low hardness of PMMA. Future improvements that combine the scratch resistance of chemically strengthened glasses, with the scalability and mechanics of PMMA/glass nacre composites may result in a material with ideal mechanical and durable optical properties. These strategies demonstrate that truly transparent, rather than translucent, tough, and strong glass composites are not only feasible but improving yearly. Future challenges in bioinspired composites will likely incorporate connective phases that are capable of "healing" postfracture,[283–285] or that can change their mechanical or optical properties under external stimuli.[286,287]

9. Summary and Outlook

The study of glass mechanics offers exciting challenges and opportunities toward new material design and applications. In particular, thin and ultrathin glasses suitable as flexible substrates, microstructured devices, surface layers or structural and functional components in advanced devices, present a promising field of exploration. In the last several years, glass chemical research has revealed a surprising number of new avenues for glass design, from glass-forming hybrids with organic and inorganic components to high-entropy oxides, hydrated materials, bioinspired materials, and glass formulation

assisted by computational resources and machine-learning algorithms. While these new developments hold great promise toward the next generation of glass applications, their further advancement will require in depth understanding of structure–mechanical property relations and their tailoring through compositional adjustments and postprocessing. This includes the development of modeling tools with improved predictive power.

To this end, new insight into the nature of glassy disorder and the elucidation of physical descriptors and quantifiers for the statistics of elastic fluctuations require their transfer from today's computational models to real-world materials. Machine learning will require physical descriptors instead of simple compositional data, which can be obtained from simultaneous advances in computational and analytical or phenomenological research. Some specific challenges include

i) in situ characterization of stress/strain fields and transient, as well as permanent, structural rearrangements during loading in both experiment and simulation, including the direct imaging of elastic fluctuations in experimental scenarios,
ii) experimental advances in environmental and vacuum studies of glass mechanics, including material characterization at variable length scale, temperature, observation time, and loading conditions,
iii) a shift in focus from mean-field approximations to the fundamental role of structural disorder, spatial and temporal fluctuations, and medium-range-order structural features, including elucidation of their tailorability through adjustments of chemical composition and thermomechanical history,
iv) studies across extended length and time scales, for example, relations between nanoscale deformation and macroscale fracture,
v) experimental demonstration of tailored disorder, including order-in-disorder, disorder-in-order, disorder-in-disorder material engineering,
vi) nanoscale-engineering of glasses, next-generation glass-like composites and hybrid materials which retain optical transparency and glass haptics, and
vii) demonstration of material fabrication processes, including thermal and non-thermal post-processing, fabrication of sub-µm freestanding and supported membranes and films.

In addition, surface modification by coatings and other post-processing methods remain areas that hold great opportunities for glass products with enhanced mechanical performance, in particular, in terms of early-stage defect propensity, corrosion protection, and the control of surface tribology and haptics.

In this article, we focused on the most prolific fields of study toward inorganic and hybrid glasses with visual transparency, the classical (intuitive) attribute of glassy materials. These are areas at which recent discoveries in glass physics intersect with the frontiers of glass chemistry, and where the need for glasses with enhanced mechanical performance is most obvious. While we did not comment on various other areas of interest, we note that the mechanical properties of metallic glasses, subcritical fracture and stress corrosion, or the interplay between mechanical, optical, and electrical properties offer further fields of study with exciting opportunities and challenges.

Acknowledgements

This project has received funding from the European Research Council (ERC) under the European Union's Horizon 2020 research and innovation program (L.W., grant agreements No. 681652 and 966791). M.M.S. acknowledges support from the Independent Research Fund Denmark grant no. 0136-00011B. A.E. acknowledges NSERC Discovery Grant 238913 and the Canada Research Chairs Program. E.B. acknowledges support from the Ben May Center for Chemical Theory and Computation and the Harold Perlman Family. The authors are grateful to David Richard for his help with preparing Figure 3, and to Chiara Wondraczek for providing panels (c,d) in Figure 12.

Open access funding enabled and organized by Projekt DEAL.

Conflict of Interest

The authors declare no conflict of interest.

Author Contributions

All authors jointly wrote the manuscript.

Keywords

bioinspired composites, glass, hybrid glasses, mechanical properties, oxide glass

Received: November 8, 2021
Revised: November 29, 2021
Published online: February 25, 2022

[1] R. O. Ritchie, *Nat. Mater.* **2011**, *10*, 817.
[2] L. Wondraczek, J. C. Mauro, J. Eckert, U. Kühn, J. Horbach, J. Deubener, T. Rouxel, *Adv. Mater.* **2011**, *23*, 4578.
[3] M. H. Ha, J. K. Choi, B. M. Park, K. Y. Han, *J. Mech. Sci. Technol.* **2021**, *35*, 661.
[4] A. Plichta, A. Weber, A. Habeck, *Flexible Electron. Mater. Dev. Technol.* **2003**, *769*, 273.
[5] S. Garner, S. Glaesemann, X. H. Li, *Appl. Phys. A: Mater. Sci. Process.* **2014**, *116*, 403.
[6] S. McCann, B. Singh, V. Smet, V. Sundaram, R. R. Tummala, S. K. Sitaraman, *IEEE Trans. Device Mater. Reliab.* **2016**, *16*, 622.
[7] H. C. Cheng, K. H. Li, C. Y. Shih, W. H. Chen, *IEEE Tans. Compon. Packag. Manuf. Technol.* **2018**, *8*, 2213.
[8] R. Sajzew, L. Wondraczek, *J. Am. Ceram. Soc.* **2021**, *104*, 3187.
[9] A. Reupert, J. Schröder, L. Wondraczek, *Adv. Photonics Res.* **2021**, https://doi.org/10.1002/adpr.202100104.
[10] B. P. V. Heiz, Z. Pan, G. Lautenschläger, C. Sirtl, M. Kraus, L. Wondraczek, *Adv. Sci.* **2017**, *4*, 1600362.
[11] M. Guglielmi, N. Bessegato, J. Cerdan-Diaz, K. Choju, D. Lisman, C. R. Flynn, E. Guadagnino, A. Meysner, J. Pfeifer, H. Roehl, V. Rupertus, M. Scarpa, H. Sun, J. Zhang, D. Zuccato, *Int. J. Appl. Glass Sci.* **2021**, *12*, 135.
[12] L. Cai, J. Wu, L. Lamberson, E. Streltsova, C. Daly, A. Zakharian, N. F. Borrelli, *Appl. Phys. Lett.* **2021**, *119*, 082901.
[13] Y. H. Wang, H. Jin, Q. Ma, K. Mo, H. Mao, A. Feldhoff, X. Cao, Y. Li, F. Pan, Z. Jiang, *Angew. Chem., Int. Ed.* **2020**, *59*, 4365.
[14] T. Welter, R. Mueller, J. Deubener, U. Marzok, S. Reinsch, *Front. Mater.* **2020**, *6*, 342.
[15] F. Kotz, F. Kotz, K. Arnold, W. Bauer, D. Schild, N. Keller, K. Sachsenheimer, T. M. Nargang, C. Richter, D. Helmer, B. E. Rapp, *Nature* **2017**, *544*, 337.

[16] B. P. Rodrigues, T. To, M. M. Smedskjaer, L. Wondraczek, *Rev. Mineral. Geochem.* **2022**, *87*, https://doi.org/10.2138/rmg.2021.87.07.
[17] M. M. Trexler, N. N. Thadhani, *Prog. Mater. Sci.* **2010**, *55*, 759.
[18] G. M. Camilo, *Proc. SPIE* **2003**, 4940.
[19] M. Ciccotti, *J. Phys. D: Appl. Phys.* **2009**, *42*, 214006.
[20] C. L. Rountree, *J. Appl. Phys. D* **2017**, *50*, 343002.
[21] K. S. R. Karlsson, L Wondraczek, in *Encyclopedia of Glass Science, Technology, History, and Culture*, Vol. *1* (Eds: P. Richet, R. Conradt, A. Takada, J. Dyon), Wiley, New York **2021**, pp. 391–404
[22] R. Meszaros, M. Wild, B. Merle, L. Wondraczek, *Glass Technol.: Eur. J. Glass Sci. Technol., Part A* **2011**, *52*, 190.
[23] K. W. Koch, L. Lin, J. J. Price, C. G. Kim, D. G. Moon, S. Y. Oh, J. K. Oh, J. H. Oh, C. A. Paulson, B. Zhang, A. Subramanian, A. Mayolet, C. K. Williams, S. D. Hart, *Coatings* **2020**, *10*, 1247.
[24] A. Mayolet, A. N. Subramanian, B. Zhang, C. K. Williams, C.-G. Kim, C. A. Paulson, J. J. Price, J. Amin, J.-H. Oh, K. W. Koch, L. Lin, S. D. Hart, *Opt. Lett.* **2019**, *44*, 5977.
[25] H. K. Yu, S. Oh, K. H. Choi, J. Jeon, X. Dong, S. H. Lee, J. Y. Choi, J. Akedo, J. H. Park, *Ceram. Int.* **2021**, *47*, 30531.
[26] J. Gao, H. Kim, J. Kim, J. B. Kwak, *Ceram. Int.* **2019**, *45*, 19496.
[27] C. Hühn, A. Erlebach, D. Mey, L. Wondraczek, M. Sierka, *J. Comput. Chem.* **2017**, *38*, 2349.
[28] C. R. Kurkjian, P. K. Gupta, *Phys. Chem. Glasses: Eur. J. Glass Sci. Technol., Part B* **2020**, *61*, 239.
[29] T. A. Michalske, S. W. Freiman, *J. Am. Ceram. Soc.* **1983**, *66*, 284.
[30] F. Célarié, M. Ciccotti, C. Marlière, *J. Non-Cryst. Solids* **2007**, *353*, 51.
[31] L. Wondraczek, M. Ciccotti, A. Dittmar, C. Oelgardt, F. Célarié, C. Marlière, *J. Am. Ceram. Soc.* **2006**, *89*, 746.
[32] A. Grimaldi, M. George, G. Pallares, C. Marliere, M. Ciccotti, *Phys. Rev. Lett.* **2008**, *100*, 165505.
[33] P. Kiefer, R. Balzer, J. Deubener, H. Behrens, T. Waurischk, S. Reinsch, R. Müller, *J. Non-Cryst. Solids* **2019**, *521*, 119480.
[34] P. Kiefer, J. Deubener, R. Mueller, H. Behrens, *J. Non-Cryst. Solids* **2020**, *527*, 119739.
[35] C. R. Kurkjian, P. K. Gupta, R. K. Brow, N. Lower, *J. Non-Cryst. Solids* **2003**, *316*, 114.
[36] G. Brambilla, D. N. Payne, *Nano Lett.* **2009**, *9*, 831.
[37] R. Sajzew, R. Limbach, L. Wondraczek, *Front. Mater.* **2020**, *7*, 126.
[38] G. Sani, R. Limbach, J. Dellith, İ. Sökmen, L. Wondraczek, *J. Am. Ceram. Soc.* **2021**, *104*, 3167.
[39] S. Sawamura, R. Limbach, S. Wilhelmy, A. Koike, L. Wondraczek, *J. Am. Ceram. Soc.* **2019**, *102*, 7299.
[40] T. Waurischk, S. Reinsch, T. Rouxel, H. Behrens, J. Deubener, R. Mueller, *J. Non-Cryst. Solids* **2021**, *572*, 121094.
[41] A. A. Griffith, *Philos. Trans. R. Soc., A* **1921**, *221*, 163.
[42] L. Wondraczek, *Science* **2019**, *366*, 804.
[43] T. P. Swiler, J. H. Simmons, A. C. Wright, *J. Non-Cryst. Solids* **1995**, *182*, 68.
[44] R. Limbach, K. Kosiba, S. Pauly, U. Kühn, L. Wondraczek, *J. Non-Cryst. Solids* **2017**, *459*, 130.
[45] E. J. Frankberg, J. Kalikka, F. G. Ferré, L. Joly-Pottuz, T. Salminen, J. Hintikka, M. Hokka, S. Koneti, T. Douillard, B. L. Saint, P. Kreiml, M. J. Cordill, T. Epicier, D. Stauffer, M. Vanazzi, L. Roiban, J. Akola, F. D. Fonzo, E. Levänen, K. Masenelli-Varlot, *Science* **2019**, *366*, 864.
[46] F. Angeli, O. Villain, S. Schuller, T. Charpentier, D. de Ligny, L. Bressel, L. Wondraczek, *Phys. Rev. B* **2012**, *85*, 054110.
[47] A. Wisitsorasak, P. G. Wolynes, *Proc. Nat. Acad. Sci. USA* **2012**, *109*, 16068.
[48] A. Ellison, I. A. Cornejo, *Int. J. Appl. Glass Sci.* **2010**, *1*, 87.
[49] S. Kapoor, L. Wondraczek, M. M. Smedskjaer, *Front. Mater.* **2017**, *4*, 1.
[50] M. J. Dejneka, X. Guo, J. C. Mauro, *US Patent 10494292*, **2019**.
[51] L. Wondraczek, S. Sen, H. Behrens, R. E. Youngman, *Phys. Rev. B* **2007**, *76*, 014202.
[52] S. K. Lee, P. J. Eng, H.-K. Mao, Y. Meng, M. Newville, M. Y. Hu, J. Shu, *Nat. Mater.* **2005**, *4*, 851.
[53] M.-F. Yu, O. Lourie, M. J. Dyer, K. Moloni, T. F. Kelly, R. S. Ruoff, *Science* **2000**, *287*, 637.
[54] J. Sehgal, S. Ito, *J. Am. Ceram. Soc.* **1998**, *81*, 2485.
[55] T. Rouxel, J. il Jang, U. Ramamurty, *Prog. Mater. Sci.* **2021**, *121*, 100834.
[56] K. Januchta, M. M. Smedskjaer, *J. Non-Cryst. Solids: X* **2019**, *1*, 100007.
[57] S. Yoshida, *J. Non-Cryst. Solids: X* **2019**, *1*, 100009.
[58] E. D. Cubuk, R. J. S. Ivancic, S. S. Schoenholz, D. J. Strickland, A. Basu, Z. S. Davidson, J. Fontaine, J. L. Hor, Y.-R. Huang, Y. Jiang, N. C. Keim, K. D. Koshigan, J. A. Lefever, T. Liu, X.-G. Ma, D. J. Magagnosc, E. Morrow, C. P. Ortiz, J. M. Rieser, A. Shavit, T. Still, Y. Xu, Y. Zhang, K. N. Nordstrom, P. E. Arratia, R. W. Carpick, D. J. Durian, Z. Fakhraai, D. J. Jerolmack, D. Lee, *Science* **2017**, *358*, 1033.
[59] A. Nicolas, E. E. Ferrero, K. Martens, J.-L. Barrat, *Rev. Mod. Phys.* **2018**, *90*, 045006.
[60] A. Winkelmann, O. Schott, *Ann. Phys.* **1894**, *287*, 697.
[61] A. Makishima, J. D. Mackenzie, *J. Non-Cryst. Solids* **1975**, *17*, 147.
[62] H. Liu, Z. Fu, K. Yang, X. Xu, M. Bauchy, *J. Non- Cryst. Solids* **2021**, *557*, 119419.
[63] R. C. Zeller, R. O. Pohl, *Phys. Rev. B* **1971**, *4*, 2029.
[64] V. K. Malinovsky, A. P. Sokolov, *Solid State Commun.* **1986**, *57*, 757.
[65] M. L. Falk, J. S. Langer, *Phys. Rev. E* **1998**, *57*, 7192.
[66] B. Wang, Y. Yu, M. Wang, J. C. Mauro, M. Bauchy, *Phys. Rev. B* **2016**, *93*, 064202.
[67] E. Lerner, G. Düring, E. Bouchbinder, *Phys. Rev. Lett.* **2016**, *117*, 035501.
[68] E. Lerner, E. Bouchbinder, *J. Chem. Phys.* **2021**, *155*, 200901.
[69] H. Mizuno, H. Shiba, A. Ikeda, *Proc. Natl. Acad. Sci. USA* **2017**, *114*, E97674.
[70] D. Richard, K. González-López, G. Kapteijns, R. Pater, T. Vaknin, E. Bouchbinder, E. Lerner, *Phys. Rev. Lett.* **2020**, *125*, 085502.
[71] M. A. Il'in, V. G. Karpov, D. A. Parshin, *Zh. Eksp. Teor. Fiz.* **1982**, *92*, 291.
[72] U. Buchenau, Y. M. Galperin, V. L. Gurevich, H. R. Schober, *Phys. Rev. B* **1991**, *43*, 5039.
[73] C. Rainone, E. Bouchbinder, E. Lerner, *Proc. Natl. Acad. Sci. USA* **2020**, *117*, 5228.
[74] A. Ninarello, L. Berthier, D. Coslovich, *Phys. Rev. X* **2017**, *7*, 021039.
[75] D. Richard, E. Lerner, E. Bouchbinder, *MRS Bull.* **2021**, https://doi.org/10.1557/s43577-021-00171-8.
[76] A. Marruzzo, W. Schirmacher, A. Fratalocchi, G. Ruocco, *Sci. Rep.* **2013**, *3*, 1407.
[77] G. Kapteijns, D. Richard, E. Bouchbinder, E. Lerner, *J. Chem. Phys.* **2021**, *154*, 081101.
[78] Z. Pan, O. Benzine, S. Sawamura, R. Limbach, A. Koike, T. D. Bennett, G. Wilde, W. Schirmacher, L. Wondraczek, *Phys. Rev. B* **2021**, *104*, 134106.
[79] J. Zylberg, E. Lerner, Y. Bar-Sinai, E. Bouchbinder, *Proc. Natl. Acad. Sci. USA* **2017**, *114*, 7289.
[80] J. J. Lewandowski, W. H. Wang, A. L. Greer, *Philos. Mag. Lett.* **2005**, *85*, 77.
[81] O. Benzine, S. Bruns, Z. Pan, K. Durst, L. Wondraczek, *Adv. Sci.* **2018**, *5*, 1800916.
[82] G. N. Greaves, A. L. Greer, R. S. Lakes, T. Rouxel, *Nat. Mater.* **2011**, *10*, 823.
[83] J. Ketkaew, W. Chen, H. Wang, A. Datye, M. Fan, G. Pereira, U. D. Schwarz, Z. Liu, R. Yamada, W. Dmowski, M. D. Shattuck, C. S. O'Hern, T. Egami, E. Bouchbinder, J. Schroers, *Nat. Commun.* **2018**, *9*, 3271.
[84] M. Ulizio, D. Lampman, M. Rustagi, J. Skeen, C. Walawender, *SAE Int. J. Transp. Saf.* **2017**, *5*, 47.
[85] C. I. Park, M. Seong, M. A. Kim, D. Kim, H. Jung, M. Cho, S. H. Lee, H. Lee, S. Min, J. Kim, M. Kim, J.-H. Park, S. Kwon,

B. Kim, S. J. Kim, W. Park, J.-Y. Yang, S. Yoon, I. Kang, *J. Soc. Inf. Disp.* **2018**, *26*, 287.
[86] Glass is the hidden gem in a carbon-neutral future, *Nature* **2021**, *599*, 7.
[87] P. Xu, B. Cui, Y. Bu, H. Wang, X. Guo, P. Wang, Y. R. Shen, L. Tong, *Science* **2021**, *373*, 187.
[88] D. X. Wang, J. Hauptmann, C. May, Y. J. Hofstetter, Y. Vaynzof, T. Mueller, *Flexible Printed Electron.* **2021**, *3*, 035001.
[89] Y. P. Yuan, Y. Yalikun, S. Amaya, Y. Aishan, Y. G. Shen, Y. Tanaka, *Sens. Actuators, A* **2021**, *321*, 112604.
[90] H. A. Atwater, A. R. Davoyan, O. Ilic, D. Jariwala, M. C. Sherrott, C. M. Went, W. S. Whitney, J. Wong, *Nat. Mater.* **2018**, *17*, 867.
[91] M. Vandebroek, J. Belis, C. Louter, G. Van Tendeloo, *Eng. Fract. Mech.* **2012**, *96*, 480.
[92] H. Shin, J. Noh, D. Kim, *Opt. Laser Technol.* **2021**, *138*, 106921.
[93] J. C. Mauro, *Materials Kinetics: Transport and Rate Phenomena*, Elsevier, Amsterdam **2021**.
[94] A. K. Varshneya, *Int. J. Appl. Glass Sci.* **2018**, *9*, 140.
[95] R. Tandon, S. J. Glass, *J. Eur. Ceram. Soc.* **2015**, *35*, 285.
[96] G. D. Quinn, *Int. J. Appl. Glass Sci.* **2019**, *10*, 7.
[97] S. Kooij, G. van Dalen, J. F. Molinari, D. Bonn, *Nature Commun.* **2021**, *12*, 2521.
[98] H. Lee, S. Cho, K. Yoon, J. Lee, *New J. Glass Ceram.* **2012**, *2*, 116.
[99] Z. Tang, M. B. Abrams, J. C. Mauro, N. Venkataraman, T. E. Meyer, J. M. Jacobs, X. Wu, A. J. Ellison, *Exp. Mech.* **2014**, *54*, 903.
[100] Z. Tang, M. B. Abrams, J. C. Mauro, L. R. Zoeller, N. Venkataraman, G. Hu, *Appl. Phys. A* **2014**, *116*, 471.
[101] M. M. Chaudhri, *Phys. Status Solidi* **2009**, *206*, 1410.
[102] G. Hu, J. T. Harris, Z. Tang, J. C. Mauro, *J. Non-Cryst. Solids* **2014**, *405*, 153.
[103] K. B. Broberg, *Cracks and Fracture*, Academic Press, San Diego, CA **1999**.
[104] L. B. Freund, *Dynamic Fracture Mechanics*, Cambridge University Press, Cambridge **1990**.
[105] A. Livne, E. Bouchbinder, J. Fineberg, *Phys. Rev. Lett.* **2008**, *101*, 264301.
[106] E. Bouchbinder, A. Livne, J. Fineberg, *Phys. Rev. Lett.* **2008**, *101*, 264302.
[107] E. Bouchbinder, *Phys. Rev. Lett.* **2009**, *103*, 164301.
[108] A. Livne, E. Bouchbinder, I. Svetlizky, J. Fineberg, *Science* **2010**, *327*, 1359.
[109] T. Goldman, R. Harpaz, E. Bouchbinder, J. Fineberg, *Phys. Rev. Lett.* **2012**, *108*, 104304.
[110] E. Bouchbinder, T. Goldman, J. Fineberg, *Rep. Prog. Phys.* **2014**, *77*, 046501.
[111] J. Fineberg, E. Bouchbinder, *Int. J. Fract.* **2015**, *196*, 33.
[112] C.-H. Chen, E. Bouchbinder, A. Karma, *Nat. Phys.* **2017**, *13*, 1186.
[113] Y. Lubomirsky, C.-H. Chen, A. Karma, E. Bouchbinder, *Phys. Rev. Lett.* **2018**, *121*, 134301.
[114] A. Vasudevan, Y. Lubomirsky, C.-H. Chen, E. Bouchbinder, A. Karma, *J. Mech. Phys. Solids* **2021**, *151*, 104372.
[115] E. Bouchbinder, J. Fineberg, M. Marder, *Annu. Rev. Condens. Matter Phys.* **2010**, *1*, 371.
[116] A. Livne, O. Ben-David, J. Fineberg, *Phys. Rev. Lett.* **2007**, *98*, 124301.
[117] J. Fineberg, M. Marder, *Phys. Rep.* **1999**, *313*, 1.
[118] R. Long, C.-Y. Hui, J. P. Gong, E. Bouchbinder, *Annu. Rev. Condens. Matter Phys* **2021**, *12*, 71.
[119] W. Kob, *J. Phys. Condens. Matter* **1999**, *11*, R85.
[120] J. C. Mauro, A. Tandia, K. D. Vargheese, Y. Z. Mauro, M. M. Smedskjaer, *Chem. Mater.* **2016**, *28*, 4267.
[121] M. Bauchy, *Comput. Mater. Sci.* **2019**, *159*, 95.
[122] A. K. Varshneya, J. C. Mauro, *Fundamentals of Inorganic Glasses*, 3rd ed., Elsevier, Amsterdam **2019**.
[123] S. Plimpton, *J. Comput. Phys.* **1995**, *117*, 1.
[124] J. Luo, K. D. Vargheese, A. Tandia, G. Hu, J. C. Mauro, *Sci. Rep.* **2016**, *6*, 23720.
[125] M. Wang, N. A. Krishnan, B. Wang, M. M. Smedskjaer, J. C. Mauro, M. Bauchy, *J. Non-Cryst. Solids* **2018**, *498*, 294.
[126] L. Deng, J. Du, *J. Am. Ceram. Soc.* **2019**, *120*, 2482.
[127] L. Wondraczek, S. Krolikowski, H. Behrens, *J. Non-Cryst. Solids* **2010**, *356*, 1859.
[128] L. Ding, K.-H. Lee, T. Zhao, Y. Yang, M. Bockowski, B. Ziebarth, Q. Wang, J. Ren, M. M. Smedskjaer, J. C. Mauro, *J. Am. Ceram. Soc.* **2020**, *103*, 6215.
[129] J. C. Mauro, A. Tandia, K. D. Vargheese, Y. Z. Mauro, M. M. Smedskjaer, *Chem. Mater.* **2016**, *28*, 4267.
[130] J. C. Mauro, *Curr. Opin. Solid State Mater. Sci.* **2018**, *22*, 58.
[131] K.-H. Lee, Y. Yang, B. Ziebarth, W. Mannstadt, M. J. Davis, J. C. Mauro, *J. Non-Cryst. Solids* **2020**, *528*, 119736.
[132] K.-H. Lee, Y. Yang, L. Ding, B. Ziebarth, M. J. Davis, J. C. Mauro, *J. Am. Ceram. Soc.* **2021**, *104*, 2506.
[133] K.-H. Lee, Y. Yang, L. Ding, B. Ziebarth, M. J. Davis, J. C. Mauro, *J. Am. Ceram. Soc.* **2021**, *104*, 3073.
[134] K.-H. Lee, Y. Yang, L. Ding, B. Ziebarth, M. J. Davis, J. C. Mauro, *J. Am. Ceram. Soc.* **2020**, *103*, 4295.
[135] G. N. Greaves, *J. Non-Cryst. Solids* **1985**, *71*, 203.
[136] D. A. Kilymis, J. M. Delaye, *J. Non-Cryst. Solids* **2014**, *401*, 147.
[137] D. A. Kilymis, J. M. Delaye, S. Ispas, *J. Chem. Phys.* **2016**, *145*, 044505.
[138] Z. H. Xu, X. Li, *Micro and Nano Mechanical Testing of Materials and Devices* (Eds: F. Yang, J. Li), Springer, Boston **2008**, pp. 139–153.
[139] W. Primak, *Surf. Sci.* **1969**, *16*, 398.
[140] S. A. Silling, *J. Mech. Phys. Solids* **2000**, *48*, 175.
[141] O. C. Zienkiewicz, R. L. Taylor, J. Z. Zhu, *The Finite Element Method: Its Basis and Fundamentals*, Butterworth-Heinemann, Oxford **2013**.
[142] G. Kermouche, E. Barthel, D. Vandembroucq, P. Dubujet, *Acta Mater.* **2008**, *56*, 3222.
[143] V. Keryvin, J.-X. Meng, S. Gicquel, J.-P. Guin, L. Charleux, J.-C. Sangleboeuf, P. Pilvin, T. Rouxel, G. L. Quilliec, *Acta Mater.* **2014**, *62*, 250.
[144] G. Molnár, P. Ganster, A. Tanguy, E. Barthel, G. Kermouche, *Acta Mater.* **2016**, *111*, 129.
[145] S. Bruns, T. Uesbeck, S. Fuhrmann, M. Tarragó Aymerich, L. Wondraczek, D. de Ligny, K. Durst, *J. Am. Ceram. Soc.* **2020**, *103*, 3076.
[146] S. Bruns, K. E. Johanns, H. U. R. Rehman, G. M. Pharr, K. Durst, *J. Am. Ceram. Soc.* **2017**, *100*, 1928.
[147] D. André, M. Jebahi, I. Iordanoff, J. luc Charles, J. Ô. Néauport, *Comput. Methods Appl. Mech. Eng.* **2013**, *265*, 136.
[148] E. Barthel, V. Keryvin, G. Rosales-Sosa, G. Kermouche, *Acta Mater.* **2020**, *194*, 473.
[149] J. Mehrmashhadi, M. Bahadori, F. Bobaru, *Eng. Fract. Mech.* **2020**, *240*, 107355.
[150] Y. D. Ha, F. Bobaru, *Eng. Fract. Mech.* **2011**, *78*, 1156.
[151] J. Rivera, J. Berjikian, R. Ravinder, H. Kodamana, S. Das, N. Bhatnagar, M. Bauchy, N. M. A. Krishnan, *Front. Mater.* **2019**, *0*, 239.
[152] Y. Cao, M. Kazembeyki, L. Tang, N. M. A. Krishnan, M. M. Smedskjaer, C. G. Hoover, M. Bauchy, *J. Am. Ceram. Soc.* **2021**, *104*, 3531.
[153] L. Ma, H. Xing, Q. Ding, Y. Han, Q. Li, W. Qiu, *AIP Adv.* **2019**, *9*, 015010.
[154] B. Bourdin, G. A. Francfort, J. J. Marigo, *J. Mech. Phys. Solids* **2000**, *48*, 797.
[155] J. Y. Wu, V. P. Nguyen, C. T. Nguyen, D. Sutula, S. Sinaie, S. P. A. Bordas, *Adv. Appl. Mech.* **2020**, *53*, 1.
[156] F. Freddi, L. Mingazzi, *Materials* **2020**, *13*, 3218.
[157] G. A. Rosales-Sosa, A. Masuno, Y. Higo, H. Inoue, *Sci. Rep.* **2016**, *6*, 23620.

[158] A. Makishima, J. D. Mackenzie, *J. Non-Cryst. Solids* **1973**, *12*, 35.
[159] B. Stevensson, M. Edén, *J. Non Cryst. Solids* **2013**, *378*, 163.
[160] G. A. Rosales-Sosa, A. Masuno, Y. Higo, H. Inoue, Y. Yanaba, T. Mizoguchi, T. Umada, K. Okamura, K. Kato, Y. Watanabe, *Sci. Rep.* **2015**, *5*, 15233.
[161] Y. Guo, J. Li, Y. Zhang, S. Feng, H. Sun, *iScience* **2021**, *24*, 102735.
[162] J. She, S. Sawamura, L. Wondraczek, *J. Non-Cryst. Solids: X* **2019**, *1*, 100010.
[163] G. Gao, A. Winterstein-Beckmann, O. Surzhenko, C. Dubs, J. Dellith, M. A. Schmidt, L. Wondraczek, *Sci. Rep.* **2015**, *5*, 8942.
[164] Y. Ding, K. Tanaka, L. Wondraczek, *Adv. Photonics Res.* **2021**, *2*, 2000100.
[165] Y. Kato, H. Yamazaki, S. Yoshida, J. Matsuoka, *J. Non-Cryst. Solids* **2010**, *356*, 1768.
[166] K. Januchta, R. E. Youngman, A. Goel, M. Bauchy, S. J. Rzoska, M. Bockowski, M. M. Smedskjaer, *J. Non-Cryst. Solids* **2017**, *460*, 54.
[167] K. Januchta, R. E. Youngman, A. Goel, M. Bauchy, S. L. Logunov, S. J. Rzoska, M. Bockowski, L. R. Jensen, M. M. Smedskjaer, *Chem. Mater.* **2017**, *29*, 5865.
[168] A. Winterstein-Beckmann, D. Möncke, D. Palles, E. I. Kamitsos, L. Wondraczek, *J. Non-Cryst. Solids* **2014**, *405*, 196.
[169] A. Winterstein-Beckmann, D. Möncke, D. Palles, E. I. Kamitsos, L. Wondraczek, *J. Non-Cryst. Solids* **2014**, *401*, 110.
[170] T. M. Gross, J. Wu, D. E. Baker, J. J. Price, R. Yongsunthon, *J. Non-Cryst. Solids* **2018**, *494*, 13.
[171] S. Sawamura, L. Wondraczek, *Phys. Rev. Mater.* **2018**, *2*, 092601.
[172] S. Sawamura, R. Limbach, H. Behrens, L. Wondraczek, *J. Non-Cryst. Solids* **2018**, *481*, 503.
[173] G. N. B. M. de Macedo, S. Sawamura, L. Wondraczek, *J. Non-Cryst. Solids* **2018**, *492*, 94.
[174] E. Moayedi, S. Sawamura, J. Hennig, E. Gnecco, L. Wondraczek, *J. Non-Cryst. Solids* **2018**, *500*, 382.
[175] J. Fu, H. He, W. Yuan, Y. Zhang, J. Yu, *Appl. Phys. Lett.* **2018**, *113*, 031606.
[176] B. P. Rodrigues, C. Hühn, A. Erlebach, D. Mey, M. Sierka, L. Wondraczek, *Front. Mater.* **2017**, *4*, 20.
[177] T. Rouxel, *Scr. Mater.* **2017**, *137*, 109.
[178] M. Bauchy, B. Wang, M. Wang, Y. Yu, M. J. A. Qomi, M. M. Smedskjaer, C. Bichara, F. J. Ulm, R. Pellenq, *Acta Mater.* **2016**, *121*, 234.
[179] F. Yuan, L. Huang, *Sci. Rep.* **2014**, *4*, 5035.
[180] Y. Zhang, L. Huang, Y. Shi, *Nano Lett.* **2019**, *19*, 5222.
[181] T. To, S. S. Sørensen, J. F. S. Christensen, R. Christensen, L. R. Jensen, M. Bockowski, M. Bauchy, M. M. Smedskjaer, *ACS Appl. Mater. Interfaces* **2021**, *13*, 17753.
[182] J. Luo, J. Wang, E. Bitzek, J. Y. Huang, H. Zheng, L. Tong, Q. Yang, J. Li, S. X. Mao, *Nano Lett.* **2016**, *16*, 105.
[183] K. Zheng, C. Wang, Y. Q. Cheng, Y. Yue, X. Han, Z. Zhang, Z. Shan, S. X. Mao, M. Ye, Y. Yin, E. Ma, *Nat. Commun.* **2010**, *1*, 24.
[184] L.-Q. Shen, J.-H. Yu, X.-C. Tang, B.-A. Sun, Y.-H. Liu, H.-Y. Bai, W.-H. Wang, *Sci. Adv.* **2021**, *7*, eabf7293.
[185] N. Miyata, H. Jinno, *J. Non. Cryst. Solids* **1980**, *38–39*, 391.
[186] A. K. Seal, P. Chakraborti, N. R. Roy, S. Mukherjee, M. K. Mitra, G. C. Das, *Bull. Mater. Sci.* **2005**, *28*, 457.
[187] L. Tang, N. M. Anoop Krishnan, J. Berjikian, J. Rivera, M. M. Smedskjaer, J. C. Mauro, W. Zhou, M. Bauchy, *Phys. Rev. Mater.* **2018**, *2*, 113602.
[188] J. F. S. Christensen, S. S. Sørensen, T. To, M. Bauchy, M. M. Smedskjaer, *Phys. Rev. Mater.* **2021**, *5*, 093602.
[189] F. C. Serbena, I. Mathias, C. E. Foerster, E. D. Zanotto, *Acta Mater.* **2015**, *86*, 216.
[190] B. Deng, J. Luo, J. T. Harris, C. M. Smith, T. M. Wilkinson, *Acta Mater.* **2021**, *208*, 116715.
[191] J. Deubener, M. Allix, M. J. Davis, A. Duran, T. Höche, T. Honma, T. Komatsu, S. Krüger, I. Mitra, R. Müller, S. Nakane, M. J. Pascual, J. W. P. Schmelzer, E. D. Zanotto, S. Zhou, *J. Non. Cryst. Solids* **2018**, *501*, 3.
[192] J. Amin, G. H. Beall, C. M. Smith, United States Patent, *US 9,873,631 B2*, **2018**.
[193] N. L. Clark, S.-Y. Chuang, J. C. Mauro, *J. Am. Ceram. Soc.* **2022**, *105*, 193.
[194] L. Martel, M. Allix, F. Millot, V. Sarou-Kanian, E. Véron, S. Ory, D. Massiot, M. Deschamps, *J. Phys. Chem. C* **2011**, *115*, 18935
[195] J. Luo, H. Huynh, C. G. Pantano, S. H. Kim, *J. Non-Cryst. Solids* **2016**, *452*, 93.
[196] S. M. Wiederhorn, T. Fett, G. Rizzi, M. J. Hoffmann, J. P. Guin, *Metall. Mater. Trans. A* **2013**, *44*, 1164.
[197] M. Tomozawa, E. M. Aaldenberg, *Phys. Chem. Glasses: Eur. J. Glass Sci. Technol., Part B* **2017**, *58*, 156.
[198] T. M. Gross, A. R. Sarafian, J. Wu, Z. Zheng, *US 2020/0156996 A1*, **2020**.
[199] K. Januchta, M. Stepniewska, L. R. Jensen, Y. Zhang, M. A. J. Somers, M. Bauchy, Y. Yue, M. M. Smedskjaer, *Adv. Sci.* **2019**, *6*, 1901281.
[200] T. M. Gross, G. M. Guryanov, *US 2019/0152838 A1*, **2019**.
[201] V. Venugopal, S. Sahoo, M. Zaki, M. Agarwal, N. N. Gosvami, N. M. A. Krishnan, *Patterns* **2021**, *2*, 100290.
[202] R. Ravinder, K. H. Sridhara, S. Bishnoi, H. S. Grover, M. Bauchy, Jayadeva, H. Kodamana , N. M. A. Krishnan, *Mater. Horiz.* **2020**, *7*, 1819.
[203] D. Richard, M. Ozawa, S. Patinet, E. Stanifer, B. Shang, S. A. Ridout, B. Xu, G. Zhang, P. K. Morse, J.-L. Barrat, L. Berthier, M. L. Falk, P. Guan, A. J. Liu, K. Martens, S. Sastry, D. Vandembroucq, E. Lerner, M. L. Manning, *Phys. Rev. Mater.* **2020**, *4*, 113609.
[204] E. D. Cubuk, S. S. Schoenholz, J. M. Rieser, B. D. Malone, J. Rottler, D. J. Durian, E. Kaxiras, A. J. Liu, *Phys. Rev. Lett.* **2015**, *114*, 108001.
[205] H. Liu, S. Xiao, L. Tang, E. Bao, E. Li, C. Yang, Z. Zhao, G. Sant, M. M. Smedskjaer, L. Guo, M. Bauchy, *Acta Mater.* **2021**, *210*, 116817.
[206] T. Du, H. Liu, L. Tang, S. S. Sørensen, M. Bauchy, M. M. Smedskjaer, *ACS Nano* **2021**, *15*, 17705.
[207] T. To, F. Célarié, C. Roux-Langlois, A. Bazin, Y. Gueguen, H. Orain, M. Le Fur, V. Burgaud, T. Rouxel, *Acta Mater.* **2018**, *146*, 1.
[208] U. G. K. Wegst, H. Bai, E. Saiz, A. P. Tomsia, R. O. Ritchie, *Nat. Mater.* **2015**, *14*, 23.
[209] L. L. Hench, J. K West, *Chem. Rev.* **1990**, *90*, 33.
[210] O. Mahony, O. Tsigkou, C. Ionescu, C. Minelli, L. Ling, R. Hanly, M. E. Smith, M. M. Stevens, J. R. Jones, *Adv. Funct. Mater.* **2010**, *20*, 3835.
[211] F. Tallia, L. Russo, S. Li, A. L. H. Orrin, X. Shi, S. Chen, J. A. M. Steele, S. Meille, J. Chevalier, P. D. Lee, M. M. Stevens, L. Cipolla, J. R. Jones, *Mater. Horiz.* **2018**, *5*, 849.
[212] W. Fan, R. E. Youngman, X. Ren, D. Yu, M. M. Smedskjaer, *J. Mater. Chem. B* **2021**, *9*, 4400.
[213] W. Fan, L. R. Jensen, M. Ceccato, T. S. Quaade, L. Gurevich, D. Yu, M. M. Smedskjaer, *Mater. Today Chem.* **2021**, *22*, 100584.
[214] H. Granel, C. Bossard, A.-M. Colllignon, F. Wauquier, J. Lesieur, G. Y. Rochefort, E. Jallot, J. Lao, Y. Wittrant, *ACS Appl. Bio Mater.* **2019**, *2*, 3473.
[215] T. D. Bennett, S. Horike, *Nat. Rev. Mater.* **2018**, *3*, 431.
[216] S. Horike, S. S. Nagarkar, T. Ogawa, S. Kitagawa, *Angew. Chem., Int. Ed.* **2020**, *59*, 6652.
[217] M. Liu, R. D. McGillicuddy, H. Vuong, S. Tao, A. H. Slavney, M. I. Gonzalez, S. J. L. Billinge, J. A. Mason, *J. Am. Chem. Soc.* **2021**, *143*, 2801.
[218] V. Nozari, C. Calahoo, J. M. Tuffnell, D. A. Keen, T. D. Bennett, L. Wondraczek, *Nat. Commun.* **2021**, *12*, 5703.

[219] T. D Bennett, J.-C. Tan, Y. Yue, E. Baxter, C. Ducati, N. J. Terrill, H. H.-M. Yeung, Z. Zhou, W. Chen, S. Henke, A. K. Cheetham, G. N. Greaves, *Nat. Commun.* **2015**, *6*, 8079.
[220] R. Gaillac, P. Pullumbi, K. A. Beyer, K. W. Chapman, D. A. Keen, T. D. Bennett, F.-X. Coudert, *Nat. Mater.* **2017**, *16*, 1149.
[221] C. Zhou, L. Longley, A. Krajnc, G. J. Smales, A. Qiao, I. Erucar, C. M. Doherty, A. W. Thornton, A. J. Hill, C. W. Ashling, O. T. Qazvini, S. J. Lee, P. A. Chater, N. J. Terrill, A. J. Smith, Y. Yue, G. Mali, D. A. Keen, S. G. Telfer, T. D. Bennett, *Nat. Commun.* **2018**, *9*, 5042.
[222] A. Qiao, T. D. Bennett, H. Tao, A. Krajnc, G. Mali, C. M. Doherty, A. W. Thornton, J. C. Mauro, G. N. Greaves, Y. Yue, *Sci. Adv.* **2018**, *4*, eaao6827.
[223] S. Li, R. Limbach, L. Longley, A. A. Shirzadi, J. C. Walmsley, D. N. Johnstone, P. A. Midgley, L. Wondraczek, T. D. Bennett, *J. Am. Chem. Soc.* **2018**, *141*, 1027.
[224] T. To, S. S. Sørensen, M. Stepniewska, A. Qiao, L. R. Jensen, M. Bauchy, Y. Yue, M. M. Smedskjaer, *Nat. Commun.* **2020**, *11*, 2593.
[225] L. Longley, C. Calahoo, R. Limbach, Y. Xia, J. M. Tuffnell, A. F. Sapnik, M. F. Thorne, D. S. Keeble, D. A. Keen, L. Wondraczek, T. D. Bennett, *Nat. Commun.* **2020**, *11*, 5800.
[226] T. To, S. S. Sørensen, Y. Yue, M. M. Smedskjaer, *Dalton Trans.* **2021**, *50*, 6126.
[227] M. Stepniewska, K. Januchta, C. Zhou, A. Qiao, M. M. Smedskjaer, Y. Yue, *Proc. Natl. Acad. Sci. USA* **2020**, *117*, 10149.
[228] T. D. Bennett, Y. Yue, P. Li, A. Qiao, H. Tao, G. N. Greaves, T. Richards, G. I. Lampronti, S. A. T. Redfern, F. Blanc, O. K. Farha, J. T. Hupp, A. K. Cheetham, D. A. Keen, *J. Am. Chem. Soc.* **2016**, *138*, 3484.
[229] A. Singh, M. K. Jana, D. B. Mitzi, *Adv. Mater.* **2021**, *33*, 2005868.
[230] B. K. Shaw, A. R. Hughes, M. Ducamp, S. Moss, A. Debnath, A. F. Sapnik, M. F. Thorne, L. N. McHugh, A. Pugliese, D. S. Keeble, P. Chater, J. M. Bermudez-Garcia, X. Moya, S. K. Saha, D. A. Keen, F.-X. Coudert, F. Blanc, T. D. Bennett, *Nat. Chem.* **2021**, *13*, 778.
[231] M. Parkes, F. Tallia, G. R. Young, P. Cann, J. R. Jones, J. R. T. Jeffers, *Mater. Sci. Eng. C* **2021**, *119*, 111495.
[232] S. S. Sørensen, M. B. Østergaard, M. Stepniewska, H. Johra, Y. Yue, M. M. Smedskjaer, *ACS Appl. Mater. Interfaces* **2020**, *12*, 18893.
[233] Y. Kagawa, H. Iba, M. Tanaka, H. Sato, T. Chang, *Acta Mater.* **1998**, *46*, 265.
[234] H. Iba, T. Chang, Y. Kagawa, *Compos. Sci. Technol.* **2002**, *62*, 2043.
[235] L. Wondraczek, B. Weidenfeller, G. Heide, G. H. Frischat, G. Ziegmann, *Glass Sci. Technol.* **2003**, *76*, 3, 103.
[236] S. E. Naleway, M. M. Porter, J. McKittrick, M. A. Meyers, *Adv. Mater.* **2015**, *27*, 5455.
[237] J. McKittrick, P. Y. Chen, L. Tombolato, E. E. Novitskaya, M. W. Trim, G. A. Hirata, E. A. Olevsky, M. F. Horstemeyer, M. A. Meyers, *Mater. Sci. Eng. C* **2010**, *30*, 331.
[238] M. Mirkhalaf, A. K. Dastjerdi, F. Barthelat, *Nat. Commun.* **2014**, *5*, 3166.
[239] F. Barthelat, H. Tang, P. Zavattieri, C. Li, H. Espinosa, *J. Mech. Phys. Solids* **2007**, *55*, 306.
[240] A. P. Jackson, J. F. V. Vincent, R. M. Turner, *Compos. Sci. Technol.* **1989**, *36*, 255.
[241] B. L. Smith, T. E. Schäffer, M. Viani, J. B. Thompson, N. A. Frederick, J. Kindt, A. Belcher, G. D. Stucky, D. E. Morse, P. K. Hansma, *Nature* **1999**, *399*, 761.
[242] A. G. Evans, Z. Suo, R. Z. Wang, I. A. Aksay, M. Y. He, J. W. Hutchinson, *J. Mater. Res.* **2001**, *16*, 2475.
[243] F. Barthelat, C.-M. Li, C. Comi, H. D. Espinosa, *J. Mater. Res.* **2006**, *21*, 1977.
[244] F. Song, Y. L. Bai, *J. Mater. Res.* **2003**, *18*, 1741.
[245] H. D. Espinosa, J. E. Rim, F. Barthelat, M. J. Buehler, *Prog. Mater. Sci.* **2009**, *54*, 1059.
[246] P. Fratzl, O. Kolednik, F. D. Fischer, M. N. Dean, *Chem. Soc. Rev.* **2016**, *45*, 252.
[247] I. Jäger, P. Fratzl, *Biophys. J.* **2000**, *79*, 1737.
[248] B. Ji, H. Gao, *J. Mech. Phys. Solids* **2004**, *52*, 1963.
[249] C. Jiang, V. V. Tsukruk, *Adv. Mater.* **2006**, *18*, 829.
[250] I. Corni, T. J. Harvey, J. A. Wharton, K. R. Stokes, F. C. Walsh, R. J. K. Wood, *Bioinspiration Biomimetics* **2012**, *7*, 031001.
[251] Z. Tang, N. A. Kotov, S. Magonov, B. Ozturk, *Nat. Mater.* **2003**, *2*, 413.
[252] P. Podsiadlo, A. K. Kaushik, E. M. Arruda, A. M. Waas, B. S. Shim, J. Xu, H. Nandivada, B. G. Pumplin, J. Lahann, A. Ramamoorthy, N. A. Kotov, *Science* **2007**, *318*, 80.
[253] L. J. Bonderer, A. R. Studart, L. J. Gauckler, *Science* **2008**, *319*, 1069.
[254] P. Podsiadlo, A. K. Kaushik, B. S. Shim, A. Agarwal, Z. Tang, A. M. Waas, E. M. Arruda, N. A. Kotov, *J. Phys. Chem. B* **2008**, *112*, 14359.
[255] T. Ebina, F. Mizukami, *Adv. Mater.* **2007**, *19*, 2450.
[256] P. Das, S. Schipmann, J.-M. Malho, B. Zhu, U. Klemradt, A. Walther, *ACS Appl. Mater. Interfaces* **2013**, *5*, 3738.
[257] J. Wang, Q. Cheng, L. Lin, L. Chen, L. Jiang, *Nanoscale* **2013**, *5*, 6356.
[258] J. Wang, Q. Cheng, L. Lin, L. Jiang, *ACS Nano* **2014**, *8*, 2739.
[259] U. G. K. Wegst, M. Schecter, A. E. Donius, P. M. Hunger, *Philos. Trans. R. Soc., A* **2010**, *368*, 2099.
[260] S. Deville, E. Maire, G. Bernard-Granger, A. Lasalle, A. Bogner, C. Gauthier, J. Leloup, C. Guizard, *Nat. Mater.* **2009**, *8*, 966.
[261] E. Munch, M. E. Launey, D. H. Alsem, E. Saiz, A. P. Tomsia, R. O. Ritchie, *Science* **2008**, *322*, 1516.
[262] S. Deville, *Materials* **2010**, *3*, 1913.
[263] S. Deville, E. Saiz, A. P. Tomsia, *Acta Mater.* **2007**, *55*, 1965.
[264] Q. Fu, M. N. Rahaman, F. Dogan, B. S. Bal, *J. Biomed. Mater. Res., Part B* **2008**, *86B*, 514.
[265] E. Munch, E. Saiz, A. P. Tomsia, S. Deville, *J. Am. Ceram. Soc.* **2009**, *92*, 1534.
[266] K. Lebreton, J. M. Rodríguez-Parra, R. Moreno, M. I. Nieto, *Adv. Appl. Ceram.* **2015**, *114*, 296.
[267] T. Waschkies, R. Oberacker, M. J. Hoffmann, *J. Am. Ceram. Soc.* **2009**, *92*, S79.
[268] J.-W. Moon, H.-J. Hwang, M. Awano, K. Maeda, *Mater. Lett.* **2003**, *57*, 1428.
[269] H. Bai, Y. Chen, B. Delattre, A. P. Tomsia, R. O. Ritchie, *Sci. Adv.* **2015**, *1*, e1500849.
[270] Y. Zhang, L. Hu, J. Han, *J. Am. Ceram. Soc.* **2009**, *92*, 1874.
[271] M. M. Porter, P. Niksiar, J. McKittrick, *J. Am. Ceram. Soc.* **2016**, *99*, 1917.
[272] M. M. Porter, M. Yeh, J. Strawson, T. Goehring, S. Lujan, P. Siripasopsotorn, M. A. Meyers, J. McKittrick, *Mater. Sci. Eng. A* **2012**, *556*, 741.
[273] M. N. Cooke, J. P. Fisher, D. Dean, C. Rimnac, A. G. Mikos, *J. Biomed. Mater. Res.* **2003**, *64B*, 65.
[274] R. C. R. Gergely, S. J. Pety, B. P. Krull, J. F. Patrick, T. Q. Doan, A. M. Coppola, P. R. Thakre, N. R. Sottos, J. S. Moore, S. R. White, *Adv. Funct. Mater.* **2015**, *25*, 1043.
[275] S. J. Kalita, S. Bose, H. L. Hosick, A. Bandyopadhyay, *Mater. Sci. Eng. C* **2003**, *23*, 611.
[276] L. S. Dimas, G. H. Bratzel, I. Eylon, M. J. Buehler, *Adv. Funct. Mater.* **2013**, *23*, 4629.
[277] D. Kokkinis, M. Schaffner, A. R. Studart, *Nat. Commun.* **2015**, *6*, 8643.
[278] T. Magrini, F. Bouville, A. R. Studart, *Open Ceram.* **2021**, *6*, 100109.
[279] Z. Yin, A. Dastjerdi, F. Barthelat, *Acta Biomater.* **2018**, *75*, 439.
[280] Z. Yin, F. Hannard, F. Barthelat, *Science* **2019**, *364*, 1260.
[281] T. Magrini, S. Moser, M. Fellner, A. Lauria, F. Bouville, A. R. Studart, *Adv. Funct. Mater.* **2020**, *30*, 2002149.

[282] A. Amini, A. Khavari, F. Barthelat, A. J. Ehrlicher, *Science* **2021**, *373*, 1229.
[283] G. Du, A. Mao, J. Yu, J. Hou, N. Zhao, J. Han, Q. Zhao, W. Gao, T. Xie, H. Bai, *Nat. Commun.* **2019**, *10*, 800.
[284] Y. Wang, X. Huang, X. Zhang, *Nat. Commun.* **2021**, *12*, 1.
[285] N. J. Kanu, E. Gupta, U. K. Vates, G. K. Singh, *Composites, Part A* **2019**, *121*, 474.
[286] X. Xia, A. Afshar, H. Yang, C. M. Portela, D. M. Kochmann, C. V. Di Leo, J. R. Greer, *Nature* **2019**, *573*, 205.
[287] H. Meng, G. Li, *Polymer* **2013**, *54*, 2199.

Lothar Wondraczek is professor of glass chemistry and Director of the Otto Schott Institute of Materials Research at the Friedrich Schiller University Jena. Previously, he was a professor of materials science at the University of Erlangen-Nuremberg (2008–2012), and a senior research scientist at Corning's European Technology Center (2005–2008). He holds a Dr.-Ing. from Clausthal University of Technology. His research interests involve glasses and other types of disordered materials, from chemical formulation to post-processing and the design of prototype devices.

Eran Bouchbinder is a full professor of physics at the Department of Chemical and Biological Physics, Weizmann Institute of Science, and the Director of the Ben May Center for Chemical Theory and Computation. He completed his Ph.D. in physics at Weizmann Institute of Science in 2007 and his postdoctoral training at the Hebrew University of Jerusalem in 2009. His research focuses on developing theories of various nonequilibrium, spatially extended phenomena in condensed-matter physics, materials physics, statistical physics, geophysics and biophysics.

Allen Ehrlicher is the Canada Research Chair in active biological mechanics and an associate professor of bioengineering at McGill University. He received his Ph.D. in physics from the University of Leipzig working with Josef Käs. He was then a postdoctoral researcher at Harvard University and Medical School. Dr. Ehrlicher joined the faculty of McGill in 2013 where he helped to build the Department of Bioengineering. For the last two decades, he has studied active mechanics in biology; how these systems generate, respond to, and resist forces in diverse contexts. The applications range from human health and pathology to bioinspired strong composites.

John C. Mauro is professor of materials science and engineering at The Pennsylvania State University. John earned a B.S. in glass engineering science, B.A. in computer science, and Ph.D. in glass science, all from Alfred University. His expertise is in glass science, condensed matter physics, thermodynamics and kinetics, and the topology of disordered networks. He joined Corning Incorporated in 1999, and the faculty at Penn State in 2017. John is a Fellow of the National Academy of Inventors, the American Ceramic Society, and the Society of Glass Technology.

Roman Sajzew earned B.Sc. and M.Sc. degrees in materials science from the Friedrich Schiller University Jena. Currently, he is a Ph.D. candidate at the Otto Schott Institute of Materials Research. His research interests range from thin-film synthesis and characterization to micromechanical investigation of brittle materials and methods for glass strengthening.

Morten M. Smedskjaer is a professor of materials chemistry and Head of the Doctoral Program in biotechnology, chemistry, and environmental Engineering at the Department of Chemistry and Bioscience, Aalborg University. He received his Ph.D. degree from the same university in 2011, with research stays at National University of Singapore and Zhejiang University. He worked as a research scientist at Corning Inc. from 2011 to 2012. His current research interests include the structure, dynamics, and mechanical properties of oxide and hybrid glasses, which are studied using a combination of experimental and computational methods.